Article

SOURCE DATA | TRANSPARENT PROCESS

THE EMBO JOURNAL

Relief of hypoxia by angiogenesis promotes neural stem cell differentiation by targeting glycolysis

Christian Lange[1,2], Miguel Turrero Garcia[3], Ilaria Decimo[1,2], Francesco Bifari[1,2], Guy Eelen[1,2], Annelies Quaegebeur[1,2], Ruben Boon[1,2], Hui Zhao[4,5], Bram Boeckx[4,5], Junlei Chang[6], Christine Wu[6], Ferdinand Le Noble[7,8], Diether Lambrechts[4,5], Mieke Dewerchin[1,2], Calvin J Kuo[6], Wieland B Huttner[3] & Peter Carmeliet[1,2,*]

Abstract

Blood vessels are part of the stem cell niche in the developing cerebral cortex, but their *in vivo* role in controlling the expansion and differentiation of neural stem cells (NSCs) in development has not been studied. Here, we report that relief of hypoxia in the developing cerebral cortex by ingrowth of blood vessels temporo-spatially coincided with NSC differentiation. Selective perturbation of brain angiogenesis in vessel-specific Gpr124 null embryos, which prevented the relief from hypoxia, increased NSC expansion at the expense of differentiation. Conversely, exposure to increased oxygen levels rescued NSC differentiation in Gpr124 null embryos and increased it further in WT embryos, suggesting that niche blood vessels regulate NSC differentiation at least in part by providing oxygen. Consistent herewith, hypoxia-inducible factor (HIF)-1α levels controlled the switch of NSC expansion to differentiation. Finally, we provide evidence that high glycolytic activity of NSCs is required to prevent their precocious differentiation *in vivo*. Thus, blood vessel function is required for efficient NSC differentiation in the developing cerebral cortex by providing oxygen and possibly regulating NSC metabolism.

Keywords hypoxia; neural stem cell; neurogenesis; stem cell metabolism; vascular niche

Subject Categories Neuroscience; Vascular Biology & Angiogenesis

DOI 10.15252/embj.201592372 | Received 23 June 2015 | Revised 22 December 2015 | Accepted 5 January 2016 | Published online 8 February 2016

The EMBO Journal (2016) 35: 924–941

See also: **JM Morante-Redolat & I Fariñas** (May 2016)

Introduction

Radial glia (RGs) in the ventricular zone (VZ) of the developing cerebral cortex (simply referred to as "cortex") are neural stem cells (NSCs) that generate neurons and glia in the cortex during development. RGs switch from expansion to generation of neurons by traversing from a symmetric division (producing two RGs) to an asymmetric division, mostly generating one RG plus one basal progenitor (BP; also termed intermediate progenitor cell, IPC), a committed neurogenic progenitor (Gotz & Huttner, 2005; Kriegstein & Alvarez-Buylla, 2009). The timing and extent of the switch from RG expansion to BP generation and, thus, neurogenesis determines the number of neurons in the cortex and their cellular identity in the cortical layers (Franco & Muller, 2013). Thus, proper regulation of RG expansion *versus* differentiation safeguards cortical development and prevents developmental disorders, associated with epilepsy, autism, and schizophrenia (Sun & Hevner, 2014), but the underlying signals and mechanisms are incompletely understood.

Radial glia differentiation is regulated by signals from the cortical stem cell niche (Johansson *et al*, 2010; Bjornsson *et al*, 2015). In various developing organs, blood vessels are an essential component of stem cell niches that regulate the balance between precursor expansion and differentiation (Cleaver & Dor, 2012; Ramasamy *et al*, 2015). For the brain, co-culturing embryonic NSCs with immortalized endothelial cells *in vitro* increases NSC expansion and directs their fate toward neurons (Shen *et al*, 2004). *In vivo*, the pattern of angiogenesis in the cortex seems to correlate with the initiation of neurogenesis (Miyama *et al*, 1997; Shen *et al*, 2004), but conclusive evidence for an interrelation is lacking. Further, vessels attract newborn BPs in the VZ and induce their division in the vicinity of vessels (Javaherian & Kriegstein, 2009; Stubbs *et al*, 2009) and impaired vessel formation by deletion of VEGF reduces neural precursor cell (NPC) proliferation and survival, but direct

1 Laboratory of Angiogenesis and Neurovascular Link, Vesalius Research Center, VIB, Leuven, Belgium
2 Laboratory of Angiogenesis and Neurovascular Link, Department of Oncology, KU Leuven, Leuven, Belgium
3 Max Planck Institute of Molecular Cell Biology and Genetics, Dresden, Germany
4 Laboratory of Translational Genetics, Vesalius Research Center, VIB, Leuven, Belgium
5 Laboratory of Translational Genetics, Department of Oncology, KU Leuven, Leuven, Belgium
6 Department of Medicine, Hematology Division, Stanford University, Stanford, CA, USA
7 Angiogenesis and Cardiovascular Pathology, Max-Delbrück-Center for Molecular Medicine, Berlin, Germany
8 Department of Cell and Developmental Biology, KIT, Karlsruhe, Germany
*Corresponding author. Tel: +32 16 37 32 02; Fax: +32 16 37 25 85; E-mail: peter.carmeliet@vib-kuleuven.be

© 2016 The Authors

effects of VEGF on NPCs were not excluded (Haigh *et al*, 2003; Raab *et al*, 2004). Importantly, for all observations, the molecular mechanisms are elusive.

Signals from niche vessels have been implicated in the regulation of NSC quiescence in the adult brain (Goldman & Chen, 2011; Delgado *et al*, 2014; Ottone *et al*, 2014), and hypoxia and the hypoxia-inducible transcription factor HIF-1α have been involved in NSC proliferation and differentiation, and neuronal maturation in the adult brain (Mazumdar *et al*, 2010; Li *et al*, 2014). In contrast, the functional role of vessels and a possible function of HIF-1α in developmental neurogenesis in the embryonic brain are unclear. As the molecular mechanisms governing embryonic *versus* adult NSC expansion and differentiation differ (Urban & Guillemot, 2014), and embryonic NSCs rely on rapid proliferation for expansion, while adult NSCs rely on long periods of quiescence for self-renewal (Kippin *et al*, 2005; Lange *et al*, 2009), it is unknown whether vessels and HIF-1α in the embryonic NSC niche exert a similar or distinct function as in the adult niches. Mediators of HIF-1α in NSC regulation also remain to be identified.

HIF-1α regulates glycolytic metabolism (Iyer *et al*, 1998), but only circumstantial evidence suggests a role of metabolism in NSC fate regulation. *Drosophila* neuroblasts switch from anaerobic metabolism to oxidative phosphorylation during development, and induction of oxidative phosphorylation is required for cell cycle exit and differentiation of neuroblasts (Homem *et al*, 2014). Similarly, adult mammalian NSCs *in vitro* increase oxygen consumption upon differentiation and inhibition of the electron transport chain increases proliferation (Wang *et al*, 2010; Bartesaghi *et al*, 2015). However, it is unknown whether NPC metabolism is altered in the *in vivo* niche during mammalian brain development, and whether alteration of metabolism alone functionally regulates NSC differentiation.

Thus, it remains unclear whether and how niche vessels influence NPC proliferation and cell fate during prenatal brain development *in vivo,* and whether they regulate this process by supplying oxygen. We therefore characterized the role of blood vessels in regulating neurogenesis in the developing cerebral cortex.

Results

Angiogenesis is linked to neurogenesis during cortical development

Previous studies documented the onset of angiogenesis and neurogenesis during cortical development (Miyama *et al*, 1997; Shen *et al*, 2004), but their temporo-spatial relationship has never been established side-by-side in the same study. Thus, we stained the developing mouse cerebral cortex for the endothelial marker isolectin B4 (IB4), the neurogenic marker Ngn1 (Kim *et al*, 2011), specific for both differentiating RGs and newborn BPs, and the BP marker Tbr2 (Englund *et al*, 2005) during cortical development (see Appendix Fig S1 for scheme). We found a striking temporo-spatial congruence of intraparenchymal vessel formation and induction of RG differentiation. At E10.5, vessels were absent and only single, scattered $Ngn1^+$ and $Tbr2^+$ NPCs were present in the cortex (Fig EV1A and B). In contrast, by E11.5, vessels had formed in the lateral but not the dorsal cortex, accompanied by an increase in $Ngn1^+$ and $Tbr2^+$ NPCs in the lateral but not the avascular dorsal cortex (Fig EV1C and D). One day later at E12.5, vessels had now also formed in the dorsal cortex, together with a higher number of $Ngn1^+$ and $Tbr2^+$ NPCs at this location as compared to E11.5 (Fig EV1F and G). Similar results were obtained when using the *Tis21*-GFP mouse model, which labels all neurogenic NPCs (Haubensak *et al*, 2004) (Fig EV1E and H). The pattern of angiogenesis was confirmed using CD31 as endothelial marker (Fig EV1I–K). These data reveal a close temporo-spatial correlation between blood vessel formation and the switch to neurogenesis *in vivo*.

We also studied neuron formation from proliferating precursors in the context of vessel ingrowth in the cortex. EdU was injected in pregnant mice at E10.5 or E11.5 and 24 h later, the EdU^+ progeny of the proliferating precursors that initially incorporated the label was identified as proliferating precursors by the presence of the proliferation marker Ki67, while postmitotic neurons were Ki67-negative. When EdU was injected at E10.5 and the EdU^+ progeny was analyzed at E11.5 (over a time window when vessels form in the lateral cortex), formation of $EdU^+/Ki67^-$ neurons was lower in the avascular dorsal than vascularized lateral cortex (Fig EV1L–Q). When EdU was injected at E11.5 and the analysis was performed at E12.5, the rate of neurogenesis was not changed in the lateral cortex but threefold more $EdU^+/Ki67^-$ neurons were detected in the newly vascularized dorsal cortex, when compared to E11.5 (Fig EV1N–Q).

The neocortex has undergone substantial evolutionary expansion in mammals, implicating changes in the regulation of neural precursor expansion and differentiation between lissencephalic (mouse) and gyrencephalic (ferret) species. We thus investigated whether vessel formation and RG differentiation were also congruent in the ferret cortex at developmental stages corresponding to E10.5, E11.5, and E12.5 of mouse development, that is, E20, E24, and E28 in the ferret (Noctor *et al*, 1997). Staining of vessels with IB4 and BPs with Tbr2 revealed a similar pattern of angiogenesis and BP generation as seen in the mouse cortex, that is, the congruence of increased generation of BPs in the VZ from RGs and cortex vascularization at E20 (Fig EV2A–C,), E24 (Fig EV2D–F), and E28 (Fig EV2H–I). These results identified a conserved correlation between angiogenesis and the induction of RG differentiation in the cortex in lissencephalic and gyrencephalic brains. Together, these data revealed a tight temporo-spatial link between blood vessel formation and the switch from NPC expansion to neurogenesis in the developing cortex.

Perturbing periventricular vessel ingrowth causes cortical hypoxia and impairs neurogenesis

To investigate a possible requirement of angiogenesis for the switch of NPCs from expansion to neurogenesis, we studied cortical development in homozygous Gpr124 LacZ knock-in null ($Gpr124^{KO}$) embryos, which show central nervous system (CNS)-restricted impairment and perturbation of angiogenesis in the forebrain and ventral spinal cord, but not in peripheral organs (Kuhnert *et al*, 2010; Anderson *et al*, 2011; Cullen *et al*, 2011). Gpr124 is an Wnt7a/b-specific co-activator of Wnt signaling in CNS endothelial cells (Zhou & Nathans, 2014). Since Gpr124 expression in the developing CNS is restricted to endothelial cells and pericytes (Kuhnert *et al*, 2010; Anderson *et al*, 2011; Cullen *et al*, 2011), the effect of global Gpr124 deficiency is blood vessel specific in the brain. Since $Gpr124^{KO}$ embryos are embryonic lethal from E15.5 on (Kuhnert

© 2016 The Authors

et al, 2010), we used these embryos until E13.5 to exclude general effects of embryonic morbidity.

Consistent with previous reports (Kuhnert *et al*, 2010; Anderson *et al*, 2011; Cullen *et al*, 2011), the normal periventricular vascular plexus was nearly completely absent, and only disorganized vascular tufts were formed in the ventral forebrain and neocortex, but not in the cortical hem (Fig 1A and B, asterisk) of Gpr124^{KO} embryos at E13.5. Wild-type (WT) and heterozygous-deficient littermates were indistinguishable (together referred to as controls). Staining for the hypoxia marker pimonidazole revealed increased levels of hypoxia, and neuroepithelial expression of the hypoxia-inducible gene *Glut1* was elevated in the cortex of E13.5 Gpr124^{KO} embryos (Appendix Fig S2A–D).

Suppression of periventricular vessel ingrowth inhibits the switch from RG expansion to neurogenesis

Gpr124^{KO} brains showed notably wider and thinner cortices, a hallmark of increased RG expansion (Farkas *et al*, 2008; Siegenthaler *et al*, 2009). We thus measured the lateral extension of the neocortex marked by Pax6 expression, between its border with the cortical hem (Fig 1C and D, arrowhead) and the border between the neocortex and lateral ganglionic eminence (Fig 1C and D, arrow). Notably, lateral extension of the cortex was increased in Gpr124^{KO} embryos, indicative of increased RG expansion (Fig 1E).

To assess whether inhibition of brain angiogenesis in Gpr124^{KO} embryos affected neurogenesis, we injected EdU at E12.5 and analyzed the cellular identity of EdU$^+$ cells at E13.5. The proportion of EdU$^+$/Ki67$^-$ newborn neurons was lower in Gpr124^{KO} than WT embryos, while correspondingly the proportion of EdU$^+$/Ki67$^+$ precursors in the VZ was increased (Fig 1F–H). Thus, suppression of vessel formation inhibits neurogenesis and increases NSC expansion.

To explore whether changes in the RG or BP population were underlying the reduced neurogenesis in Gpr124^{KO} as compared to WT embryos, we stained for the cortical RG marker Pax6 and the BP marker Tbr2. The total proportion of newborn RG-derived BPs, migrating through the VZ at E13.5, was decreased in Gpr124^{KO} embryos (Fig 1I–K). Importantly, all Tbr2$^-$ cells in the VZ expressed Pax6, identifying them as RGs (Fig 1I and J). In addition, we performed birthdating of newborn BPs by EdU injection at E13.5, and after an 8-h chase to allow division of the labeled cells, we counted only newly generated EdU$^+$ BPs in the VZ (Appendix Fig S2E–J). EdU$^+$ BPs in the VZ were approaching but had not reached the subventricular zone (SVZ) in WT and Gpr124^{KO} embryos, enabling us to distinguish them from the EdU$^+$ progeny of preexisting BPs in the SVZ. Strikingly, the fraction of EdU$^+$ VZ cells that were newborn RG-derived BPs was reduced in Gpr124^{KO} brains (Appendix Fig S2K), confirming that RGs generate fewer BPs upon perturbation of brain angiogenesis.

To further investigate whether the switch of RGs, BPs, or both NPCs from expansion to neurogenesis was impaired in Gpr124^{KO} embryos, we quantified the proportion of neurogenic RGs (Ngn1$^+$/Tbr2$^-$) and newborn neurogenic BPs (Ngn1$^+$/Tbr2$^+$) in the cortical VZ at E13.5. While the proportion of neurogenic Ngn1$^+$/Tbr2$^+$ BPs was only insignificantly reduced, the neurogenic Ngn1$^+$/Tbr2$^-$ RG population was strikingly reduced in Gpr124^{KO} embryos (Fig 1L–N). Consequently, the proportion of expanding RGs that are Ngn1$^-$/Tbr2$^-$ was increased (Fig 1L–O). Since Ngn1 is only present during the G1 phase of the cell cycle (Britz *et al*, 2006), we confirmed our findings in Gpr124^{KO} and control embryos expressing *Tis21*-GFP, which is present in all neurogenic NPCs. The proportions of both neurogenic *Tis21*-GFP$^+$ BPs and RGs were reduced in Gpr124^{KO} embryos compared to controls, while that of expanding RGs (Tbr2$^-$*Tis21*-GFP$^-$) was enlarged (Fig 1P–S). In addition, we confirmed that apoptosis in the cortex was low and not altered by Gpr124 deletion (Appendix Fig S2L). Together, suppression of vessel formation in Gpr124^{KO} embryos reduced neurogenesis and RG differentiation.

Inhibition of brain angiogenesis does not change BP fate

We then investigated whether the fate of BPs was changed upon perturbation of brain angiogenesis by quantifying the expression of the neurogenic markers Ngn1 and *Tis21*-GFP in the BP population. The proportion of Ngn1$^+$/Tbr2$^+$ as well as *Tis21*-GFP$^+$/Tbr2$^+$ BPs in the VZ was similar in control and Gpr124^{KO} BPs (Appendix Fig S2M and N), suggesting that cell fate of the BPs was not altered after

Figure 1. Suppression of brain angiogenesis expands radial glia cells.

A, B Immunostaining for CD31$^+$ blood vessels in control (ctrl, A) and Gpr124^{KO} (B) forebrains. Note the normal vasculature in the cortical hem (asterisk) of Gpr124^{KO} mice.

C, D Immunostaining for Pax6 in control (C) and Gpr124^{KO} (D) forebrains to reveal the lateral extension of the neocortex (dashed line) between the cortical hem (arrowhead) and the lateral ganglionic eminence (arrow).

E Quantification of the lateral extension of the cortex in control and Gpr124^{KO} brains (mean ± SEM; $N = 10$; ***$P < 0.001$).

F, G Staining for EdU (red) and Ki67 (green) in control (F) and Gpr124^{KO} (G) cortices at E13.5, 24 h after EdU injection.

H Quantification of Ki67$^+$ NPCs in the VZ (blue), SVZ/CP (gray) and of Ki67$^-$ neurons (cyan) generated from EdU-labeled NPCs in control and Gpr124^{KO} embryos (mean ± SEM; $N = 4$ (control) and $N = 3$ (Gpr124^{KO}); *$P < 0.05$, **$P < 0.01$).

I, J Immunostaining for Tbr2 (red) and Pax6 (green) in control (I) and Gpr124^{KO} (J) cortices.

K Quantification of newborn BPs in the VZ of control and Gpr124^{KO} cortices (mean ± SEM; $N = 4$; *$P < 0.05$).

L, M Immunostaining for Tbr2 (red) and Ngn1 (green) in control (L) and Gpr124^{KO} (M) cortices.

N, O Quantification of neurogenic (Ngn1$^+$) RGs and BPs (N) or expanding (Tbr2$^-$ Ngn1$^-$) RGs (O) in control and Gpr124^{KO} cortices (mean ± SEM; $N = 4$; *$P < 0.05$, ***$P < 0.001$). Note that the fraction of total BPs is significantly reduced (see K), while the fraction of Ngn1$^+$ BPs is insignificantly reduced (Fig 1N), because the proportion of Ngn1$^+$ Tbr2$^+$ cells within all BPs is slightly, though statistically insignificantly higher in the Gpr124^{KO} brains (see Appendix Fig S2M).

P, Q Stainings for Tbr2 (red) and for *Tis21*-GFP expression (green) in control (P) and Gpr124^{KO} (Q) cortices.

R, S Quantification of neurogenic (*Tis21*-GFP$^+$) RGs and BPs (R) or expanding (Tbr2$^-$ *Tis21*-GFP$^-$) RGs (S) in control and Gpr124^{KO} cortices (mean ± SEM; $N = 4$; ***$P < 0.001$).

Data information: Full, dotted, and dashed lines indicate basal and apical boundaries of the cortex or the basal boundary of the VZ, respectively. CP, cortical plate; IZ, intermediate zone; SVZ, subventricular zone; and VZ, ventricular zone. Scale bars: 250 μm (B, D) or 50 μm (G, J, M, Q), respectively.

 © 2016 The Authors

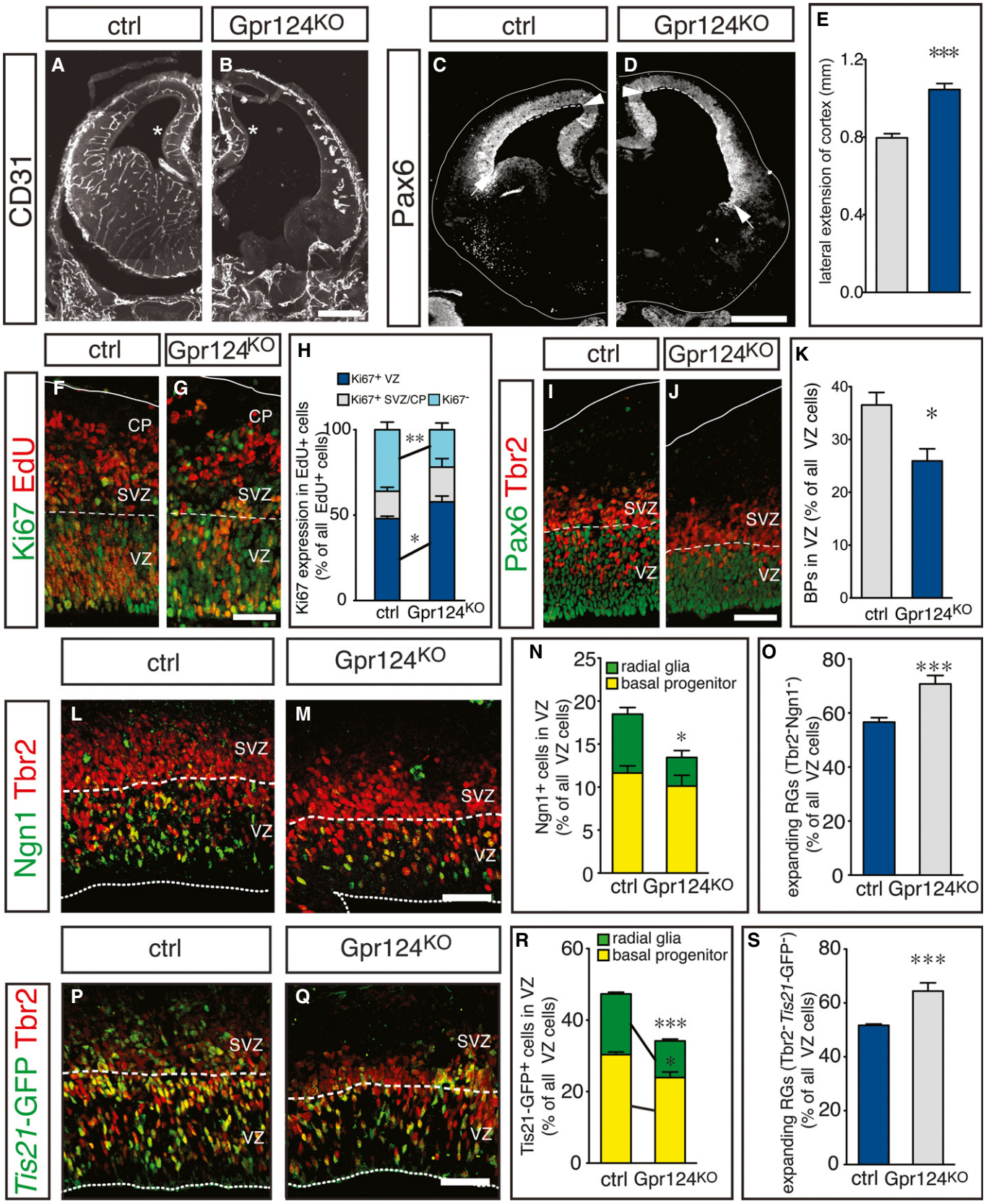

Figure 1.

© 2016 The Authors

inhibition of brain angiogenesis and that the regulation of the switch to neurogenesis by angiogenesis occurred most likely at the level of RGs rather than BPs.

Vascular deletion of Gpr124 is sufficient for increased RG expansion

To exclude the possibility that non-vascular changes were responsible for the increased RG expansion in $Gpr124^{KO}$ brains, we generated embryos with an endothelial-specific deletion of Gpr124 ($Gpr124^{ECcKO}$), by intercrossing the endothelial cell-selective PDGFB-Cre^{ERT2} line with $Gpr124^{KO/lox}$ mice and injecting tamoxifen at E10.5. The vascular phenotype of the conditional deletion was milder than that of the germ line deletion (Fig 2A and B), likely due to delayed onset of the loss of Gpr124 function after tamoxifen injection. However, the vascular defects were sufficient to cause hypoxia in the cortical VZ, as evidenced by pimonidazole staining (Fig 2C and D). Similar to $Gpr124^{KO}$ brains, the lateral extension of the cortex was also increased in $Gpr124^{ECcKO}$ brains (Fig 2E–G) and we also found a decrease in the generation of neurons, but more EdU^+/$Ki67^+$ cells were maintained in the VZ (Fig 2H–J). Moreover, the abundance of neurogenic $Ngn1^+$ RGs and newborn BPs was decreased in the VZ in $Gpr124^{ECcKO}$ brains as compared to Cre-negative controls (Fig 2K–N), while the proportion of expanding ($Tbr2^-$/$Ngn1^-$) RGs was increased (Fig 2K–O). Thus, suppression of brain angiogenesis alone by selective deletion of Gpr124 in endothelial cells was sufficient to impair the switch from RG expansion to differentiation, the generation of BPs and ultimately neurogenesis.

HIF-1α regulates the differential gene expression in $Gpr124^{KO}$ NPCs

To obtain insight into the molecular mechanisms underlying the increased RG expansion in the absence of functional vessels in the cortex, we performed transcriptional profiling via RNA-Seq of freshly sorted VZ cells from $Gpr124^{KO}$ or control embryos. Prominin1-positive ($Prom1^+$) cells from the VZ (Weigmann *et al*, 1997) and Prominin1-negative ($Prom1^-$) cells from the SVZ and neuronal layers were MACS-sorted from dissociated WT cortices at E14.5, and expression of cell differentiation markers was analyzed by qRT–PCR. RG-specific transcripts *Fabp7* and *Hes5* were highly enriched in the $Prom1^+$ fraction (12.4- and 23.1-fold, respectively), while the neuronal transcripts *Dcx* and *Tubb3* were depleted (threefold), indicating that sorting for Prom1 enriched VZ cells (Fig 3A).

We then sequenced mRNA of $Prom1^+$ sorted VZ cells from $Gpr124^{KO}$ or control embryos. Gene expression profiling revealed that transcript levels of 252 genes were upregulated and 253 genes were downregulated by more than 1.5-fold in the avascular $Gpr124^{KO}$ VZ with a false discovery rate < 0.05 (Appendix Fig S3A). Analysis of gene ontology terms using DAVID software revealed a strong enrichment of genes involved in glucose metabolism (glycolysis), angiogenesis, and cell proliferation among the upregulated genes in NSCs from $Gpr124^{KO}$ cortices, while importantly genes functioning in neurogenesis were most enriched among the downregulated genes (Fig 3B and C). Further, we used Ingenuity pathway analysis (www.ingenuity.com) to identify transcription factors, whose targets were enriched among the regulated genes, therefore likely being candidate gene regulators in NSCs from the $Gpr124^{KO}$ cortex. This analysis identified several targets of the transcriptional mediators of hypoxia HIF-1α and HIF-2α as the most significantly enriched among the genes with increased expression, while targets of Tbr2 and the oncogene Bmi1 were most enriched among the genes with decreased expression, consistent with decreased differentiation (Fig 3D and E).

To confirm HIF activation in the $Gpr124^{KO}$ cortex, we performed immunoblotting for HIF-1α and HIF-2α in control and $Gpr124^{KO}$ brains, and found a strong induction of HIF-1α abundance in $Gpr124^{KO}$ as compared to control brains, while HIF-2α was undetectable (Fig 3F and G). Immunostaining for HIF-1α revealed the presence of HIF-1α in extranuclear speckles in the control, but strongly increased abundance and nuclear localization in the $Gpr124^{KO}$ cortex (Fig 3H–I''). Moreover, increased expression of prototypical HIF target genes in the $Gpr124^{KO}$ cortex was confirmed by qRT–PCR (Fig 3J). Importantly, classical target genes of the Wnt pathway and the Notch pathway, the two master regulators of RG expansion (Johansson *et al*, 2010; Pierfelice *et al*, 2011), were not changed (Appendix Fig S3B–E). Other target genes of the Wnt-mediator β-catenin were even enriched among the genes downregulated in $Gpr124^{KO}$ NPCs (Fig 3E). Thus, the increased RG expansion in the $Gpr124^{KO}$ cortex was associated with activation of the HIF pathway, independently of the Wnt and Notch pathways.

Figure 2. Blood vessels intrinsically control radial glia expansion.

A, B Staining for isolectin $B4^+$ blood vessels in control (A) and $Gpr124^{ECcKO}$ (B) forebrains. Asterisks mark the lateral ventricles.

C, D Staining for pimonidazole (PIMO, green) and isolectin $B4^+$ blood vessels (red) in control (C) and $Gpr124^{ECcKO}$ (D) cortices.

E, F Immunostaining for Pax6 in control (E) and $Gpr124^{ECcKO}$ (F) forebrain sections to reveal the lateral extension of the neocortex (dashed line) between the cortical hem (arrowhead) and the lateral ganglionic eminence (arrow).

G Quantification the lateral extension of the cortex in control and $Gpr124^{ECcKO}$ brains (mean ± SEM; $N = 6$ for ctrl and $N = 8$ for $Gpr124^{ECcKO}$; $^*P < 0.05$).

H, I Staining for EdU (red) and Ki67 (green) in control (H) and $Gpr124^{ECcKO}$ (I) cortices at E13.5, 24 h after EdU injection.

J Quantification of $Ki67^+$ NPCs in the in VZ (blue), SVZ/CP (gray), and of $Ki67^-$ neurons (cyan) generated from EdU-labeled NPCs in control and $Gpr124^{ECcKO}$ embryos (mean ± SEM; $N = 4$; $^*P < 0.05$, $^{**}P < 0.01$).

K, L Immunostaining for Tbr2 (red) and Ngn1 (green) in control (K) and $Gpr124^{KO}$ (L) cortices.

M–O Quantification of neurogenic ($Ngn1^+$) RGs and BPs (M), newborn BPs (N), or expanding ($Tbr2^-$ $Ngn1^-$) RGs (O) in control and $Gpr124^{ECcKO}$ cortices (mean ± SEM; $N = 4$; $^*P < 0.05$, $^{**}P < 0.01$). Note that the fraction of total BPs is significantly reduced (N), while the fraction of $Ngn1^+$ BPs is insignificantly reduced (M), because the proportion of $Ngn1^+$ $Tbr2^+$ cells within all BPs is slightly, though statistically insignificantly higher in the $Gpr124^{KO}$ brains (not shown).

Data information: Full, dotted, and dashed lines indicate basal and apical boundaries of the cortex or the basal boundary of the VZ, respectively. CP, cortical plate; IZ, intermediate zone; SVZ, subventricular zone; and VZ, ventricular zone. Scale bars: 100 μm (B, D, F) or 50 μm (I, L).

 © 2016 The Authors

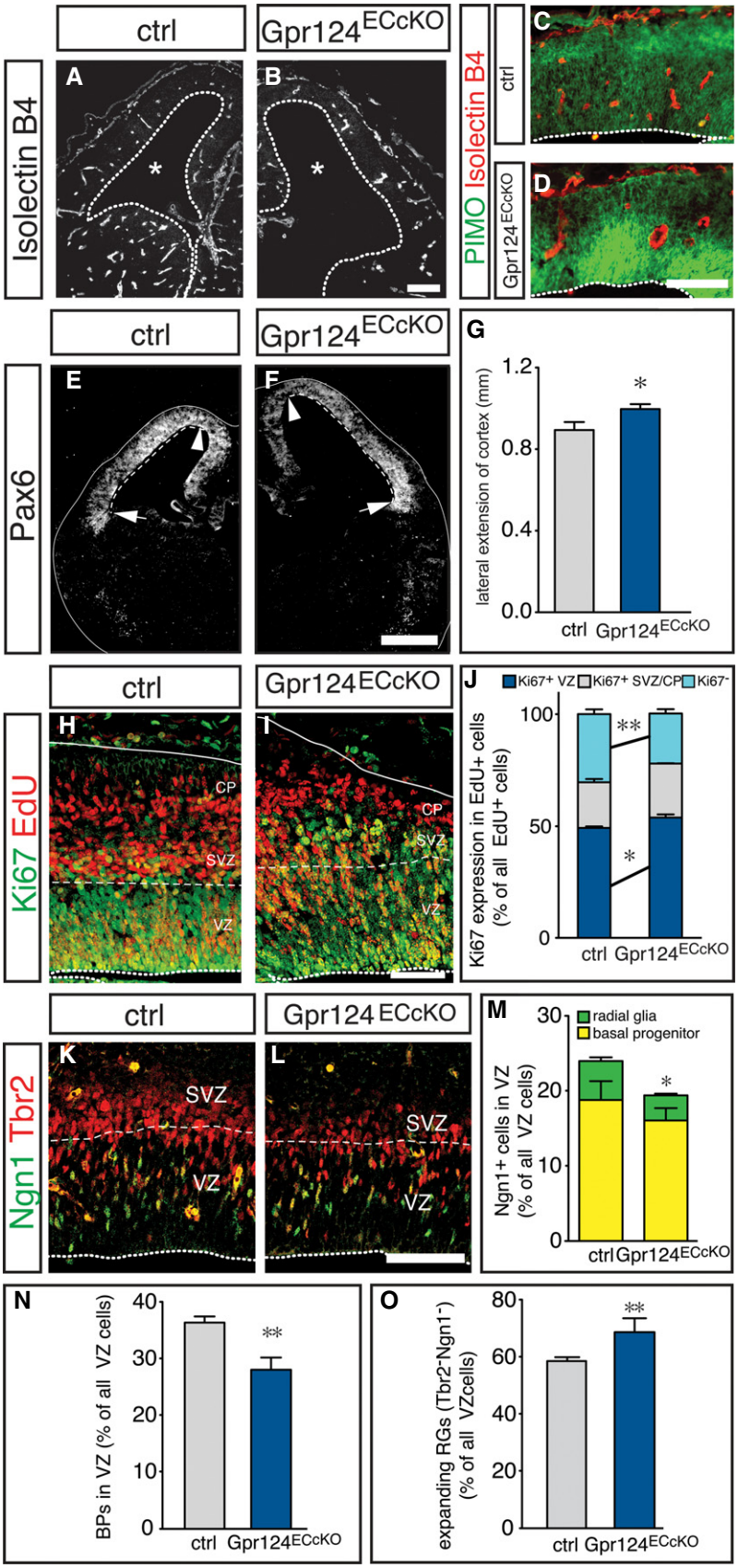

Figure 2.

© 2016 The Authors

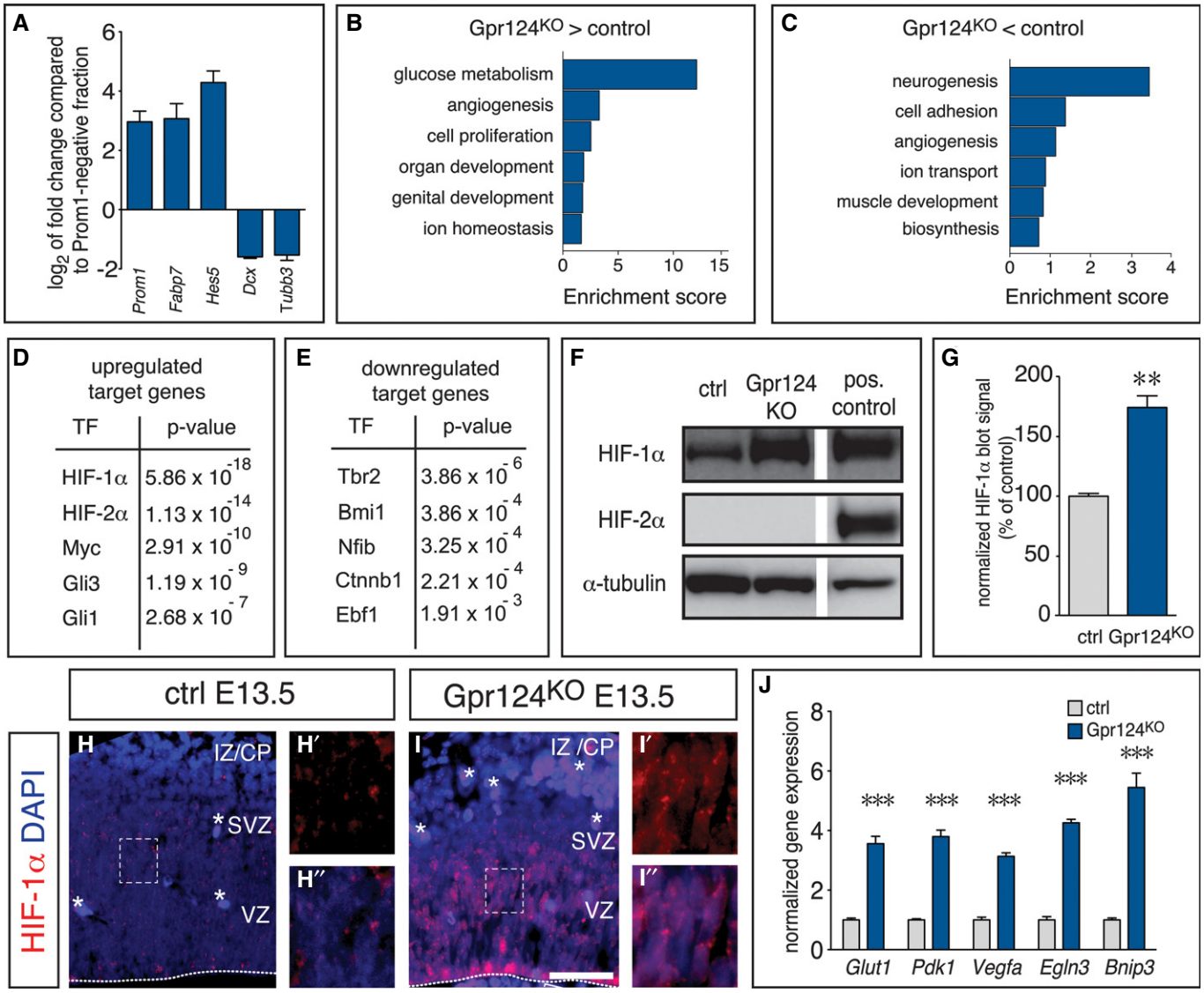

Figure 3. HIF-1α is the main regulator of the differential gene expression pattern in Gpr124^{KO} NPCs.

A qRT–PCR analysis of NSC-specific markers (*Fabp7*, *Hes5*) and neuronal markers (*Dcx*, *Tubb3*) in the Prom1^{+} fraction, presented as fold change compared to the Prom1^{-} fraction) from WT cortices at E14.5 (mean ± SEM; $N = 3$ for *Dcx*; $N = 6$ for all other genes).

B, C Enrichment analysis for biological process gene ontology terms associated with the genes upregulated (B) or downregulated (C) in VZ cells from Gpr124^{KO} embryos.

D, E Enrichment analysis showing the *P*-value of the target enrichment for upstream transcriptional regulators known to control the expression of the genes that were upregulated (D) or downregulated (E) in Prom1^{+} VZ cells from Gpr124^{KO} as compared to control cortex.

F Western blot for HIF-1α (top), HIF-2α (middle) and α-tubulin as loading control (bottom) using forebrain lysates from E13.5 control (left) or Gpr124^{KO} embryos (middle). HIF-1/2α-transfected HEK293 cells served as positive control (right).

G Quantification of HIF-1α band intensities shown in (F) (mean ± SEM; $N = 3$; $^{**}P < 0.01$).

H, I Immunostaining for HIF-1α (red) and DAPI (blue) in control (H, H', H") and Gpr124^{KO} (I,I',I") cortices. Panels (H', H", I', I") are magnifications of the boxed areas in panels (H) and (I), showing HIF-1α signal alone (H', I') or together with DAPI (H", I"). Asterisks indicate autofluorescent blood cells. The dashed line indicates the basal boundary of the VZ. Scale bar: 100 μm. CP, cortical plate; IZ, intermediate zone; SVZ, subventricular zone; and VZ, ventricular zone.

J qRT–PCR analysis of HIF-1α target gene expression in VZ cells from the cortex of control and Gpr124^{KO} E13.5 embryos (mean ± SEM; $N = 4$; $^{***}P < 0.001$).

Source data are available online for this figure.

Angiogenesis quenches HIF signaling during cortical development

Hypoxia and high HIF levels maintain stem cells *in vitro* and regulate somatic stem cells *in vivo* (Mohyeldin *et al*, 2010), but their role in RG differentiation during brain development is unclear. Considering that RG differentiation was low during cortical development when vessels were not yet formed (Fig EV1A and B'), we explored whether vessel formation in the cortex decreased HIF-dependent gene transcription by supplying oxygen. We therefore determined tissue oxygenation in the developing cortex by staining

 © 2016 The Authors

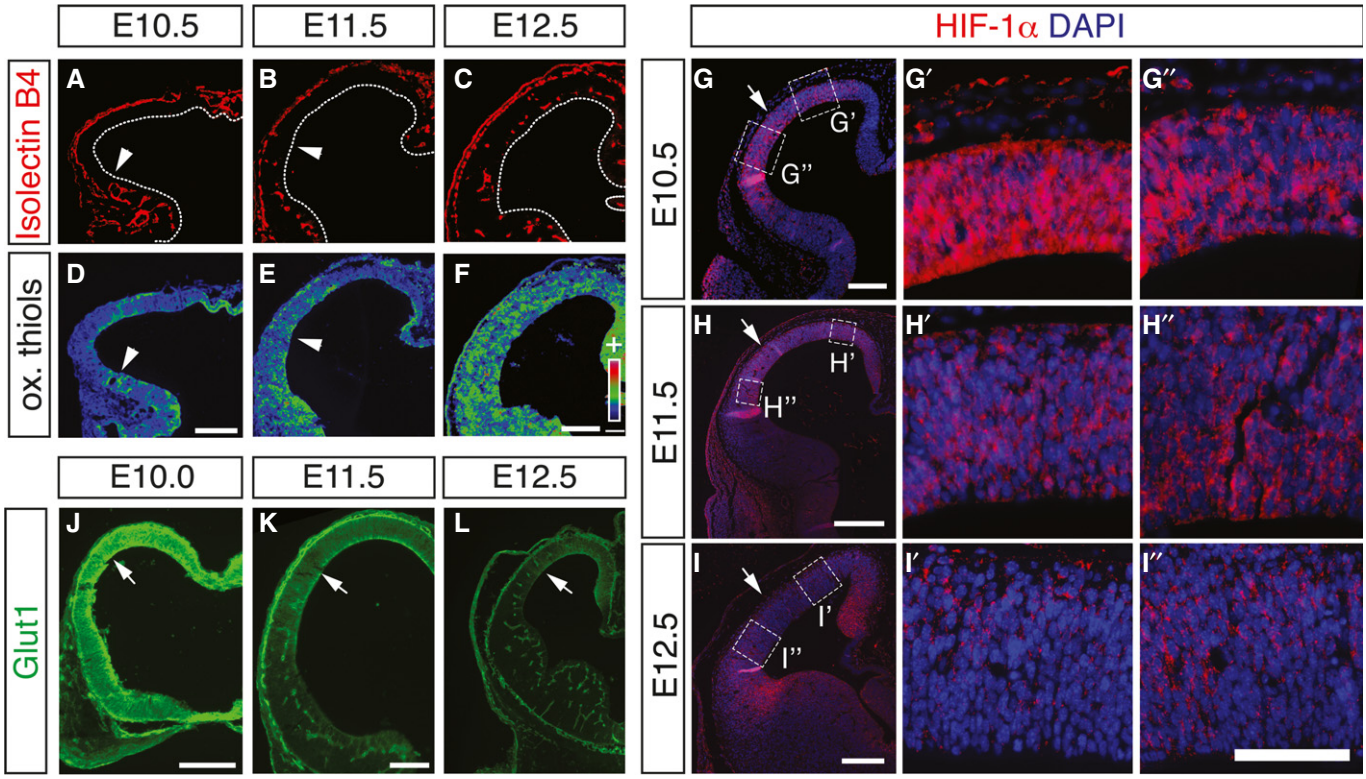

Figure 4. Angiogenesis quenches HIF activity in the developing cortex.

A–F Staining for isolectin B4 (A–C) and oxidized thiols (D–F) in WT cortices at E10.5 (A, D), E11.5 (B, E), and E12.5 (C, F). Panels (D–F) are pseudocolor conversions of staining intensity (from low [purple] to high [red]). Arrowheads denote the position of the vascular front.

G–I Immunostaining for HIF-1α (red) and DAPI (blue) in WT cortices at E10.5 (G–G″), E11.5 (H–H″), and E12.5 (I–I″). Panels (G′, G″, H′, H″, I′, I″) are magnifications of the boxed areas in their respective original panels. Arrows point to the border of lateral and dorsal cortex.

J–L Immunostaining for Glut1 of WT cortices at E10.0 (J), E11.5 (K), and E12.5 (L).

Data information: Dashed lines indicate the apical border of the cortex. Scale bars: 100 μm (D, F, G, H, I, J–L) or 50 μm (I″), respectively.

for oxidized thiols, the predominant form of cellular cysteines in well-oxygenated tissues, using an established protocol (Shah *et al*, 2011). Staining revealed lower levels of oxidized thiols in the hypoxic Gpr124^{KO} cortex than in controls, indicating that this technique indeed identified tissue hypoxia (Fig EV3A–D). During normal brain development, oxygenation was lower in the non-vascularized cortex at E10.5 than in the already vascularized ventral forebrain (Fig 4A and D), and increased in the cortex when it became vascularized (Fig 4B, C, E and F).

Moreover, we performed immunostaining for HIF-1α and the HIF target gene *Glut1*, in the developing forebrain at E10.5, E11.5, and E12.5. This analysis showed for both genes an expression pattern reciprocal to that of angiogenesis and tissue oxygenation. HIF-1α was strongly expressed and present in the nucleus of many cells in the whole E10.5 cortex and in the dorsal cortex at E11.5, but overall reduced and excluded from the nucleus concomitant with the progression of vessel formation throughout the cortex (Figs 4G–I″ and EV1I–K). Parenchymal Glut1 expression mirrored that of HIF-1α (Fig 4J–L), but Glut1 became prominently expressed in brain vessels, consistent with earlier reports (Dermietzel *et al*, 1992). Moreover, angiogenesis correlated with downregulation of the HIF target gene *Glut1* in the ferret brain parenchyma (Fig EV3E–G). *In situ* hybridization for the HIF target genes *Pdk1*, *Bnip3*, and *Mct4* *(Slc16a3)* confirmed their regulation reciprocal to the pattern of angiogenesis and HIF-1α destabilization (Appendix Fig S4). Together, vascularization increased oxygenation of the developing forebrain and reduced HIF-1α abundance and HIF target gene expression, thus linking elevated HIF transcriptional activity with suppression of RG differentiation and neurogenesis. Interestingly, tissue oxygenation was lower at E13.5 in the Gpr124^{KO} cortex than in controls (Appendix Fig S2C and D; Fig EV3A–D), and parenchymal Glut1 expression was not downregulated at E11.5 and E12.5 (Fig EV3H–K), suggesting that perturbation of brain angiogenesis counteracts the relief from initially low tissue oxygenation and high HIF activity, seen during normal brain development.

HIF-1α controls radial glia differentiation: loss-of-function

We then investigated whether HIF-1α plays a functional role in the control of RG differentiation and neurogenesis, as its role in these processes is unclear. We therefore generated embryos with conditional deletion of HIF-1α in the cerebral cortex (CC) by crossing HIF-1α$^{lox/lox}$ mice (Ryan *et al*, 2000) with Emx1-Cre mice, which induces recombination restrictedly in dorsal forebrain RGs (Gorski *et al*, 2002). Homozygous deletion of HIF-1α (HIF-1α$^{CC-/-}$) did not affect survival and fertility, but severely impaired

© 2016 The Authors

Figure 5. HIF-1α maintains radial glia during cortical development.

A qRT–PCR analysis of HIF-1α and HIF-1α target gene expression in cortices from E13.5 WT and HIF-1α$^{CC+/-}$ embryos (mean ± SEM; $N = 8$ for WT and $N = 5$ for HIF-1α$^{CC+/-}$; $^*P < 0.05$, $^{**}P < 0.01$, $^{***}P < 0.001$).

B, C Staining for EdU (red) and Ki67 (green) in WT (B) and HIF-1α$^{CC+/-}$ (C) cortices at E13.5, 24 h after EdU injection.

D Quantification of Ki67$^+$ NPCs in the VZ (blue), SVZ/CP (gray), and of Ki67$^-$ neurons (cyan) generated from EdU-labeled NPCs in control and HIF-1α$^{CC+/-}$ brains (mean ± SEM; $N = 4$; $^*P < 0.05$).

E, F Immunostaining for Tbr2 (red) and Ngn1 (green) in WT (E) or HIF-1α$^{CC+/-}$ (F) cortices at E13.5.

G–I Quantification of neurogenic (Ngn1$^+$) RGs and BPs (G), newborn BPs (H), or expanding (Tbr2$^-$ Ngn1$^-$) RGs (I) in control and HIF-1α$^{CC+/-}$ cortices at E13.5 (mean ± SEM; $N = 5$; $^*P < 0.05$, $^{**}P < 0.01$, $^{***}P < 0.001$).

J Whole mount image of brains from WT or HIF-1α$^{CC+/-}$ mice at P5.

K Quantification of cortex area in brain sections from P5 WT or HIF-1α$^{CC+/-}$ mice (mean ± SEM; $N = 8$ (WT) or $N = 6$ (HIF-1α$^{CC+/-}$); $^*P < 0.05$).

L, M Staining with Hoechst 33248 in P5 WT (L) or HIF-1α$^{CC+/-}$ (M) cortices. The double arrow denotes the measured thickness of the cortex.

N Quantification of cortical thickness of WT and HIF-1α$^{CC+/-}$ cortices (mean ± SEM; $N = 8$ (WT) or $N = 6$ (HIF-1α$^{CC+/-}$); $^{***}P < 0.001$).

O–Q Epifluorescent images of the E16.5 cortex, 3 days after *in utero* electroporation (IUE) with EGFP alone (ctrl, O), wild-type HIF-1α+EGFP (P) or mutant HIF-1αΔC+EGFP (Q). Panels (O', P', Q') are magnifications of the boxed area in their respective original panel.

R Quantification of EGFP$^+$ cells in the cortical zones VZ/SVZ, IZ, and CP shown in (O–Q) (mean ± SEM; $N = 5$; $^*P < 0.05$).

S–U qRT–PCR analysis of NSC marker (S; mean ± SEM; $N = 5$; $^*P < 0.05$), neurogenic markers (T; mean ± SEM; $N = 5$; $^*P < 0.05$, $^{***}P < 0.001$), and HIF target genes (U; mean ± SEM; $N = 5$; $^*P < 0.05$, $^{**}P < 0.01$) in expanding NPCs (eNPCs) and neurogenic NPCs (nNPCs). Gene expression was normalized to the levels in eNPCs.

Data information: Full, dotted, and dashed lines indicate basal and apical boundaries of the cortex or the boundaries of the cortical zones, respectively. CP, cortical plate; IZ, intermediate zone; SVZ, subventricular zone; and VZ, ventricular zone. Scale bars: 50 μm (C, F, Q'), 200 μm (M, Q), or 4 mm (J), respectively.

angiogenesis in the cerebral cortex (where Cre is expressed) and caused cortical hypoplasia together with apoptosis in the cortical parenchyma (Fig EV4A–D'), suggesting that parenchymal HIF-1α expression is required for vessel formation in the cortex. We therefore analyzed NPC differentiation in embryos, lacking a single HIF-1α allele in the cerebral cortex (HIF-1α$^{CC+/-}$), which had a normal vessel density (Fig EV4E and F). qRT–PCR analysis of microdissected cortex revealed reduced expression of HIF-1α and its target genes (*Egln3, Pdk1, Glut1*) in HIF-1α$^{CC+/-}$ embryos at E13.5 (Fig 5A).

Interestingly, more neurons were generated at the expense of EdU$^+$/Ki67$^+$ VZ cells in HIF-1α$^{CC+/-}$ cortices at E13.5 ($N = 4$; $P < 0.05$; Fig 5B–D). We also found increased numbers of Ngn1$^+$ RGs (by 40%) and neurogenic BPs (by 20%), as well as an increased proportion of total newborn BPs (by 18%) in the VZ of HIF-1α$^{CC+/-}$ (Fig 5E–H). In consequence, expanding RGs (Tbr2$^-$/Ngn1$^-$) were decreased (Fig 5E–I) and apoptosis was not altered in HIF-1α$^{CC+/-}$ cortices (Fig EV4G).

Next, we investigated whether precocious RG differentiation in HIF-1α$^{CC+/-}$ brains altered cerebral cortex size in postnatal animals. Analysis of cortex size at postnatal day (P) 5 revealed a small but consistent reduction in cortex area, due to decreased cortical thickness ($N = 8$ (WT) or 6 (HIF-1α$^{CC+/-}$); $P < 0.01$; Fig 5J–N); however, the abundance of deep layer *versus* upper layer neurons was not changed (Fig EV4H–N). Together, reduction of HIF-1α expression and transcriptional activity causes precocious neurogenic differentiation of RGs and increased neurogenesis, at the expense of RG expansion, leading to mild microcephaly at postnatal stages.

HIF-1α controls radial glia differentiation: gain-of-function

We further probed the role of HIF-1α in RG differentiation by studying the effects of HIF-1α overexpression in RGs on their differentiation *in vivo*. We therefore electroporated E13.5 embryos *in utero* to selectively transfect RGs *in vivo* (Pilaz *et al*, 2009). Transfection of RGs with plasmids encoding EGFP alone (control) or together with full-length HIF-1α revealed that a larger proportion of HIF-1α-transfected RGs was maintained as NPCs in the VZ/SVZ at E16.5 compared to control-transfected cells. Moreover, the HIF-1α-transfected RGs generated fewer early-born neurons that had already reached the cortical plate, but instead more recently born neurons that were still migrating through the IZ as compared to controls (Fig 5O–P' and R), suggesting a delayed switch to differentiation by transient HIF-1α overexpression.

To distinguish a transcription dependent from a structural role of HIF-1α (e.g., by sequestering its dimerization partners Arnt and Arnt2), we used HIF-1α-ΔC (Jiang *et al*, 1997), a deletion mutant with impaired transcriptional activity (Fig EV4O). In contrast to wt HIF-1α, transfection of HIF-1α-ΔC did not significantly change RG differentiation (Fig 5Q and R). Thus, HIF-1α stabilization is critical and sufficient to maintain NPCs in an undifferentiated state and to reduce their differentiation, thereby delaying neurogenesis.

Downregulation of HIF-1α target genes during RG differentiation

To obtain more insight into the molecular mechanism of the HIF-1α-mediated prevention of precocious RG differentiation, we investigated whether the switch from RG expansion to neurogenic commitment was associated with a regulation of HIF-1α target genes. We therefore used *Tis21*-GFP mice that express GFP in neurogenic NPCs, and FACS sorted neurogenic GFP$^+$ NPCs (nNPCs) and expanding NPCs (eNPCs) as Prom1$^+$/GFP$^-$ cells. Analysis by qRT–PCR revealed higher levels of the RG marker gene *Fabp7* in expanding GFP$^-$ NPCs (Fig 5S), while neurogenic GFP$^+$ NPCs expressed higher levels of the neurogenic markers *NeuroD6, Dcx,* and *Tubb3*, confirming our sorting criteria (Fig 5T). Strikingly, expression of the HIF target genes *Egln3, Pdk1, Mct4,* and *Glut1* was reduced more than twofold in nNPCs compared to eNPCs, suggesting that the switch to neurogenesis in the cortex is linked to a downregulation of HIF target genes (Fig 5U).

Increased tissue oxygenation inhibits RG expansion in Gpr124^{KO} mice

Next, we explored whether tissue hypoxia was required for the increased RG expansion after inhibition of brain angiogenesis in Gpr124^{KO} mice. We increased tissue oxygenation in Gpr124^{KO} embryos by exposing pregnant dams to hyperoxia (80% O_2) for

 © 2016 The Authors

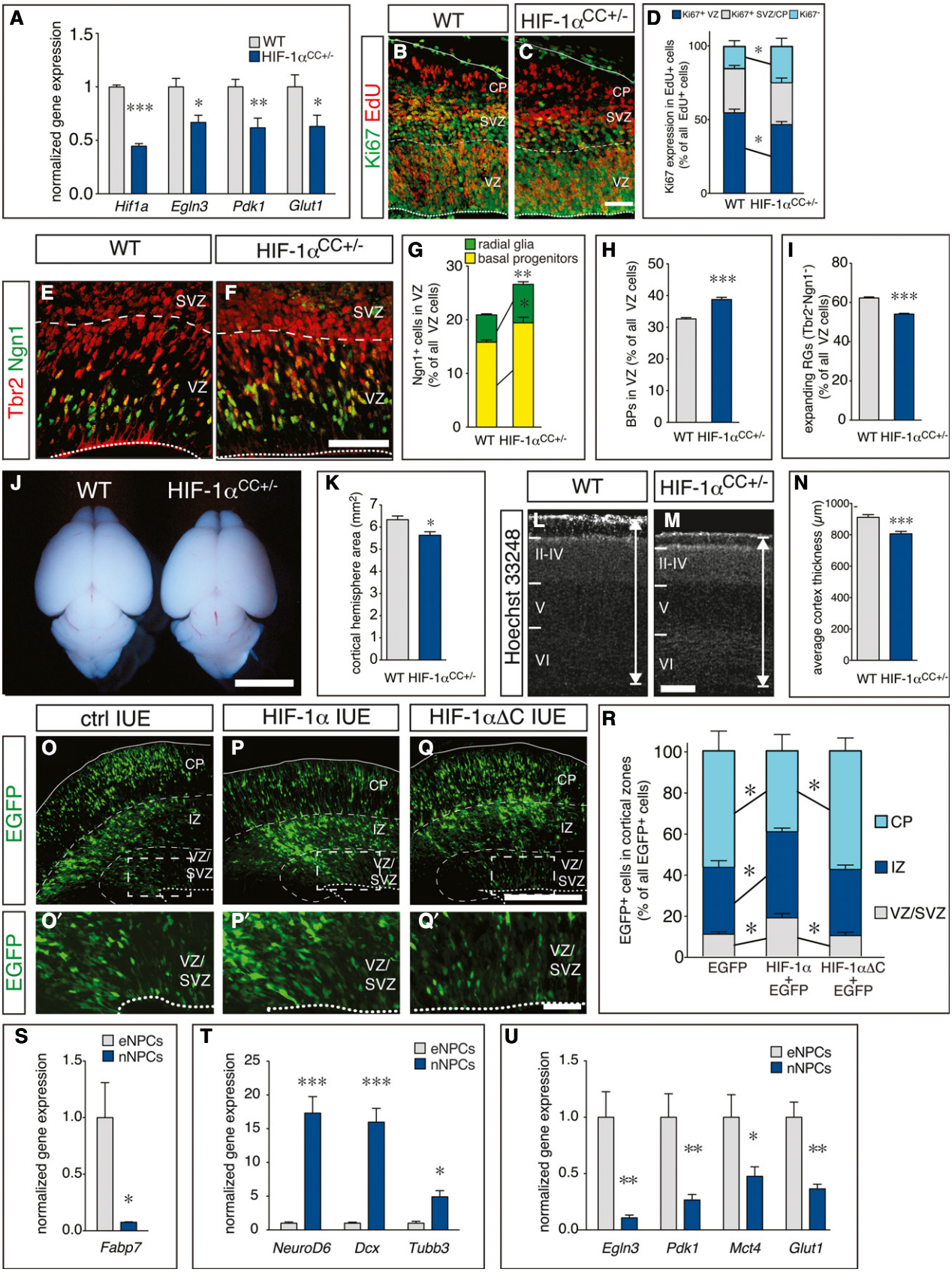

Figure 5.

© 2016 The Authors

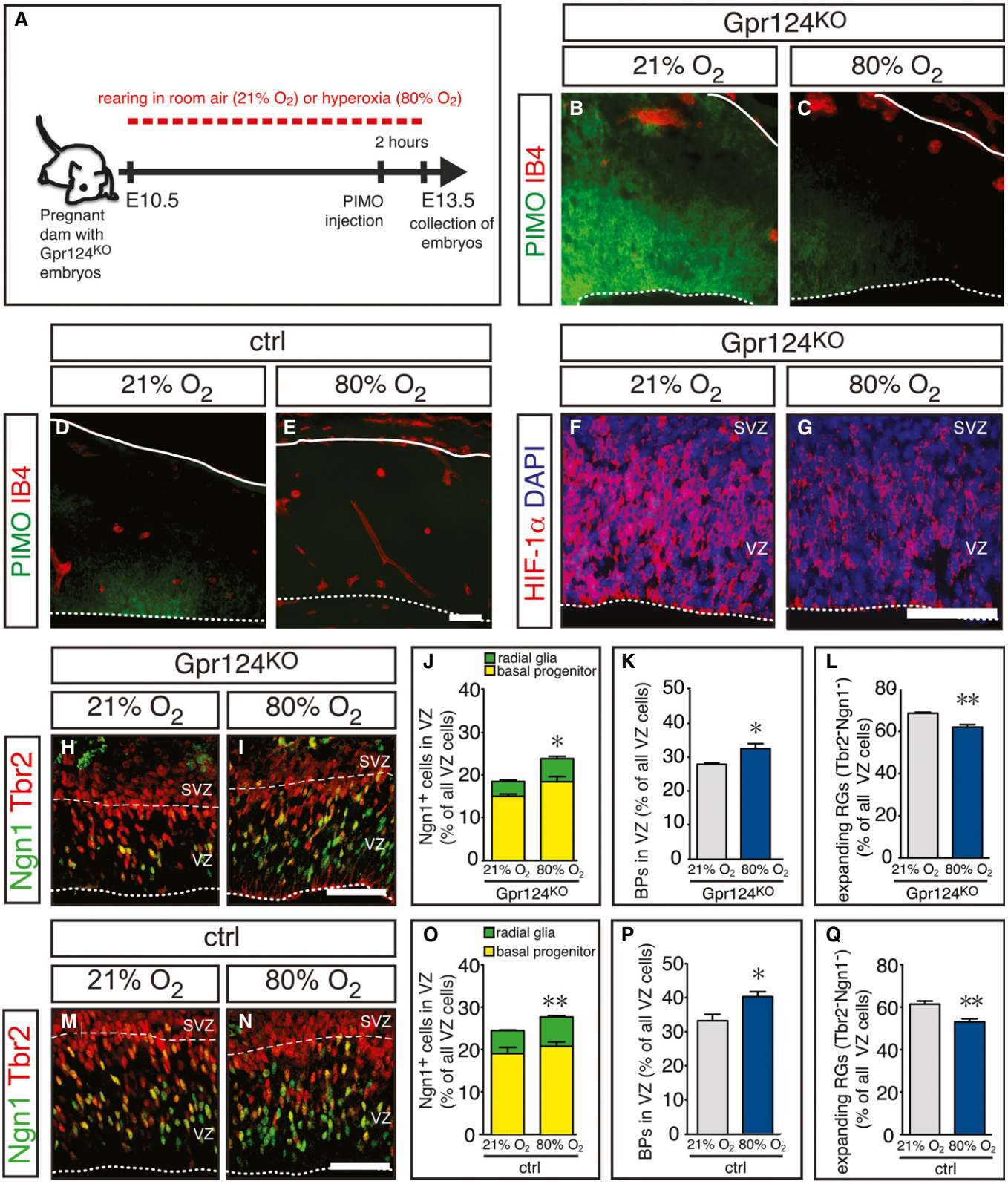

Figure 6.

3 days from E10.5 to E13.5 (Fig 6A). Hyperoxia treatment strongly reduced pimonidazole staining in the cortex of Gpr124^{KO} embryos as compared with normoxia (21% O_2) to a level comparable with control embryos, while the vascular phenotype was not changed (Fig 6B and C). Hyperoxia treatment of control embryos completely abrogated pimonidazole staining (Fig 6D and E). Similar results were

 © 2016 The Authors

Figure 6. Restoring tissue oxygenation rescues radial glia differentiation after suppression of periventricular brain angiogenesis.

A Scheme of the experimental approach.

B–E Staining for pimonidazole (PIMO, green) and isolectin B4 (IB4, red) in Gpr124^{KO} (B, C) and control (D, E) cortices after exposure of the pregnant dams to 21% O_2 (B, D) or 80% O_2 (C, E). Compared to the pimonidazole staining in panels (B, C), the intensity of this staining is much weaker in panels (D, E). For reasons of clarity, the pimonidazole staining in panels (D, E) was therefore enhanced, equally in both panels.

F, G Immunostaining for HIF-1α (red) and DAPI (blue) in Gpr124^{KO} cortices after exposure of the pregnant dams to 21% O_2 (F) or 80% O_2 (G).

H, I Immunostaining for Tbr2 (red) and Ngn1 (green) in Gpr124^{KO} cortices after exposure of the pregnant dams to 21% O_2 (H) or 80% O_2 (I).

J–L Quantification of neurogenic (Ngn1$^+$) RGs and BPs (J), newborn BPs (K), or expanding (Tbr2$^-$ Ngn1$^-$) RGs (L) in Gpr124^{KO} cortices after exposure of the pregnant dams to 21% or 80% O_2 (mean ± SEM; $N = 4$ for 21% O_2 and $N = 5$ for 80% O_2; $^*P < 0.05$, $^{**}P < 0.01$).

M, N Immunostaining for Tbr2 (red) and Ngn1 (green) in control cortices after exposure of the pregnant dams to 21% O_2 (M) or 80% O_2 (N).

O–Q Quantification of neurogenic (Ngn1$^+$) RGs and BPs (O), newborn BPs (P), or expanding (Tbr2$^-$ Ngn1$^-$) RGs (Q) in control cortices after exposure of the pregnant dams to 21% or 80% O_2 (mean ± SEM; $N = 5$; $^*P < 0.05$, $^{**}P < 0.01$).

Data information: Dotted and dashed lines indicate the basal and apical boundaries of the VZ. SVZ, subventricular zone; and VZ, ventricular zone. Scale bars: 50 μm.

obtained when staining oxidized thiols to evaluate tissue oxygenation (Appendix Fig S5). Also, hyperoxia treatment reduced HIF-1α immunostaining in the Gpr124^{KO} cortex (Fig 6F and G). These data show that exposing pregnant dams to 80% O_2 increases brain tissue oxygenation in the developing embryo and normalizes brain oxygen levels after inhibition of brain angiogenesis. Importantly, normalization of brain tissue oxygenation rescued RG differentiation in the Gpr124^{KO} cortex by increasing the proportion of neurogenic Ngn1$^+$/Tbr2$^-$ RGs (Fig 6H–J), elevating the proportion of newborn BPs in the VZ (Fig 6H–K) and reducing expanding Ngn1$^-$/Tbr2$^-$ RGs (Fig 6H–L), thus normalizing the Gpr124^{KO} phenotype. Moreover, exposure of control embryos to 80% O_2 phenocopied the effect of heterozygous HIF-1α deletion by further increasing the proportion of neurogenic Ngn1$^+$/Tbr2$^-$ RGs (Fig 6M–O) and the proportion of newborn BPs in the VZ (Fig 6M–P), while decreasing expanding Ngn1$^-$/Tbr2$^-$ RGs (Fig 6M–Q). Thus, tissue O_2 levels regulate RG expansion and normalizing oxygenation suffices to restore RG differentiation in the absence of functional brain vessels.

Glycolysis is required for RG expansion

Considering that expression of glycolytic genes was consistently increased in VZ cells of Gpr124^{KO} brains coinciding with increased RG expansion, while their expression was reduced in neurogenic as compared to expanding NPCs, we probed for a functional role of glycolysis in the regulation of RG differentiation. First, the expression of the glycolytic genes *Hk2*, *Gapdh*, *Eno1,* and *Ldha* was higher in Prom1$^+$ VZ cells than in their differentiated Prom1$^-$ progeny isolated from the E 14.5 cortex (Fig 7A).

We then measured glycolytic activity in cultured NPCs from the E13.5 cortex under expansion conditions in the presence of growth factors and upon differentiation induced by removal of growth factors. This analysis revealed that proliferating NPCs secreted large amounts of lactate (end product of glycolysis) in the conditioned medium, but lactate production was strikingly reduced already at the onset of neurogenesis after 3 days of differentiation and further decreased after 7 days of differentiation, when extensive neurogenesis and astrogliogenesis had taken place (Figs 7B and EV5A–F). These data show that glycolysis is functionally downregulated already at the switch from NSC expansion to neurogenesis *in vitro*.

To assess the functional importance of glycolysis on RG differentiation, we silenced the expression of Pfkfb3, a hypoxia-inducible activator of the rate-limiting glycolytic enzyme phosphofructokinase-1 (Pfk1). Pfkfb3 is the most abundant Pfkfb isoform in E13.5 cortical VZ cells and is upregulated in the Gpr124^{KO} VZ (Fig EV5G). Lentivirus-mediated knockdown using a scramble (scr) or Pfkfb3-specific shRNA in proliferating NPCs *in vitro* (Fig 7C) reduced lactate production (Fig 7D), but did not significantly alter total mitochondrial oxygen consumption rate (OCR) as a readout of oxidative phosphorylation (Fig 7E) or OCR dedicated to ATP production

Figure 7. High-level expression of the glycolytic regulator Pfkfb3 is required for radial glia maintenance.

A qRT–PCR analysis of glycolytic enzymes in Prom1$^+$ VZ cells and their Prom1$^-$ differentiated progeny (BPs and neurons) in WT cortices at E14.5 (mean ± SEM; $N = 3$ (*Hk2, Gapdh*); $N = 6$ (*Eno1; Ldha*); $^{**}P < 0.01$).

B Measurement of lactate secretion from proliferating NSCs, and of NSCs differentiating for 3 days (switch to neurogenesis) or for 7 days (fully differentiated), normalized to cellular protein content (mean ± SEM; $N = 6$; $^{***}P < 0.001$).

C qRT–PCR analysis of *Pfkfb3* expression in proliferating NSCs, transduced with scr or Pfkfb3 shRNA#1 (mean ± SEM; $N = 4$; $^*P < 0.05$).

D Measurement of lactate secretion from proliferating NSCs transduced with scr or Pfkfb3 shRNA#1, normalized to cellular protein content (mean ± SEM; $N = 3$; $^*P < 0.05$).

E Measurement of mitochondrial respiration rate (oxygen consumption rate, OCR_{MITO}; see Appendix Supplementary Methods) in proliferating NSCs, transduced with scr or Pfkfb3 shRNA#1, normalized to cellular protein content (mean ± SEM; $N = 3$; N.S., not significant).

F–H Epifluorescent images of the E15.5 cortex, 3 days after *in utero* electroporation with EGFP + scr shRNA (F), EGFP + Pfkfb3 shRNA#1 (G), or EGFP + Pfkfb3 shRNA#2 (H).

I Quantification of EGFP$^+$ cells in the cortical zones VZ/SVZ, IZ, and CP shown in (F–H) (mean ± SEM; $N = 4$ for scr and $N = 5$ for Pfkfb3 shRNAs; $^*P < 0.05$, $^{**}P < 0.01$, $^{***}P < 0.001$).

J–L Epifluorescent images of the mouse cortex after *in utero* electroporation with HIF-1α and scr shRNA (J) or with HIF-1α and two different Pfkfb3 shRNAs (K, L) at E16.5, 3 days after transfection.

M Quantification of EGFP$^+$ cells in the cortical zones VZ/SVZ, IZ, and CP shown in (J–L) (mean ± SEM; $N = 5$; $^*P < 0.05$, $^{**}P < 0.01$, $^{***}P < 0.001$).

Data information: Full, dotted, and dashed lines indicate basal and apical boundaries of the cortex or boundaries of the cortical zones, respectively. CP, cortical plate; IZ, intermediate zone; SVZ, subventricular zone; and VZ, ventricular zone. Scale bars: 100 μm.

© 2016 The Authors

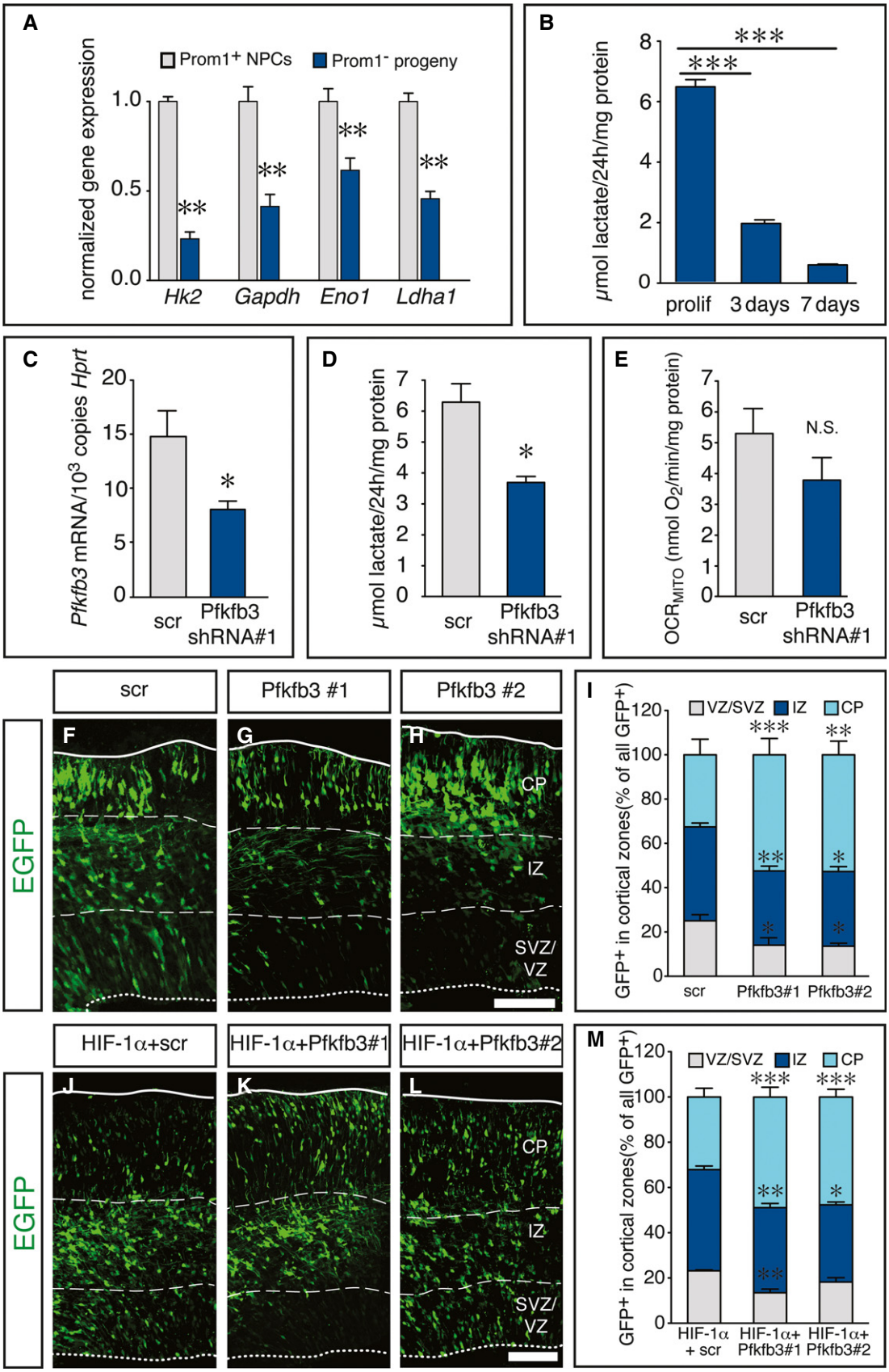

Figure 7.

© 2016 The Authors

(Fig EV5H). We silenced Pfkfb3 by *in utero* electroporation of vectors encoding EGFP together with a scr or two different non-overlapping Pfkfb3 shRNAs (Figs 7C and EV5I) at E12.5 and evaluated RG differentiation 3 days later. Silencing of Pfkfb3 strikingly reduced the proportion of transfected cells that were maintained as progenitors in the VZ/SVZ as well as the recently born neurons in the IZ, while the proportion of early-born neurons in the CP was increased (Fig 7F–I). These data indicate a critical dependence of RG expansion and/or maintenance on sufficient Pfkfb3 levels *in vivo*.

Next, we electroporated vectors encoding HIF-1α and EGFP together with a scr or Pfkfb3 shRNA in WT embryos at E13.5 and analyzed RG differentiation after 72 h. Overexpression of HIF-1α with scr shRNA reproduced the increased RG maintenance and delayed neurogenesis, seen after of HIF-1α overexpression alone (Figs 5O–R and 7J and M). However, the delay in neurogenesis was partially rescued upon Pfkfb3 silencing, as indicated by an increase of early-born neurons in the CP and a decrease of late-born neurons in the IZ (Fig 7J–M). Together, these results reveal a critical role of the hypoxia-inducible glycolytic regulator Pfkfb3 in normal and induced RG expansion after HIF-1α stabilization.

Discussion

Regulation of RG differentiation by the stem cell niche of the embryonic cerebral cortex is essential to safeguard cortical development. Our study uncovers a critical role for blood vessels as a novel functional component of this niche and identifies HIF-1α and its target Pfkfb3 as novel regulators of RG expansion during cortical development.

Blood vessels regulate radial glia expansion during development

In this study, we describe a congruence of blood vessel ingrowth and induction of RG differentiation and BP generation in the developing cerebral cortex, which is spatiotemporally propagated during cortex development. These results raised the question whether blood vessels promote RG differentiation and neurogenesis in the stem cell niche, since virtually all the cortical NSCs expanded before the vessels reached the cortex and they initiated the switch toward neuron production upon blood vessel invasion. This phenomenon was observed in both lissencephalic and gyrencephalic species, implying that it likely functions also during human brain development.

Our findings indicate that brain-specific and vessel-autonomous impairment of angiogenesis in $Gpr124^{KO}$ mouse embryos, preventing the relief of hypoxia in the initially avascular cerebral cortex, increased RG expansion and NPC proliferation, abrogated the induction of neurogenic transcription factors in RGs, and reduced the generation of BPs from these cells, thereby impairing neurogenesis, without, however, inducing apoptosis. This suggests that formation of niche blood vessels in the developing cerebral cortex regulates the switch from RG expansion to RG differentiation and neurogenesis.

These findings differ from earlier reports that deletion of VEGF in the developing CNS caused severe brain vessel defects and decreased NPC proliferation (Haigh *et al*, 2003; Raab *et al*, 2004). However, VEGF deletion in all brain cells may reduce proliferation and cause apoptosis due to severely perturbed angiogenesis, abrogating oxygen and nutrient supply, or due to lack of direct stimulation of NSC proliferation by VEGF (Jin *et al*, 2002; Kirby *et al*, 2015).

In contrast, our more refined approach of using $Gpr124^{KO}$ mice with more selective periventricular vessel defects enabled us to study the effects of perturbed niche blood vessel formation on cortical neurogenesis during development and allowed to uncover a functional dependence of neurogenesis on angiogenesis in the developing brain. Our findings show that the absence of functional blood vessels in the embryonic cortical niche does not generally impair RG function and viability but selectively causes RGs to expand *more* rather than *less*.

Oxygen tension regulates RG expansion

Blood vessels can exert their effect in the stem cell niche via angiocrine signaling or via delivery of nutrients or oxygen (Cleaver & Dor, 2012; Ramasamy *et al*, 2015). Our findings reveal that (i) initial vessel ingrowth in the cerebral cortex, coinciding with an increase in tissue oxygenation and reduced levels of HIF-1α, was associated with a reduction in RG expansion and a switch to RG differentiation; (ii) conversely, $Gpr124^{KO}$ embryos with impaired brain angiogenesis failed to increase oxygen levels in the stem cell niche and maintained RG expansion at the expense of RG differentiation; and (iii) increasing tissue oxygenation of $Gpr124^{KO}$ embryos did not alter the vascular defects, but reduced HIF-1α levels, rescued RG differentiation and normalized their expansion, while the same treatment in control embryos phenocopied the effect of partial HIF-1α deletion in the cortex.

Together, these data support a model whereby vessel ingrowth relieves the low oxygen tension in the developing cortex and degrades HIF-1α to facilitate differentiation of RGs at the expense of their expansion. Our studies do not exclude the possibility that niche blood vessels also affect neurogenesis via the production of angiocrine factors as suggested by studies *in vitro* (Shen *et al*, 2004) and in the adult NSC niche *in vivo* (Goldman & Chen, 2011; Delgado *et al*, 2014; Ottone *et al*, 2014; Bjornsson *et al*, 2015), but they suggest for a role of blood vessels in supplying oxygen as a key regulator of this process *in vivo*. In addition, none of these previous papers, which documented a role of blood vessels of the embryonic or adult NSC niche, considered that oxygen can regulate the switch from NPC expansion to differentiation, despite the fact that certain stem cells occupy hypoxic niches (Panchision, 2009; Mohyeldin *et al*, 2010). Our results therefore provide the first *in vivo* evidence that RGs expand more and differentiate less when the low oxygen levels in the early cortex fail to increase during further brain development, thereby uncovering that blood vessels regulate embryonic cortical neurogenesis at least in part by supplying oxygen.

HIF-1α integrates RG expansion and angiogenesis

Full deletion of HIF-1α in the cortex impaired angiogenesis and caused widespread apoptosis by E13.5, precluding the use of mice lacking both HIF-1α alleles. However, heterozygous deletion of HIF-1α in the cerebral cortex did not impair angiogenesis at E13.5, but still decreased the expression of HIF target genes and increased RG differentiation. Conversely, transient overexpression of HIF-1α maintained RGs and delayed their differentiation in the developing cortex, even in the presence of blood vessels. These results suggest

© 2016 The Authors

a model, whereby HIF-1α initially favors RG expansion, but at the same time also triggers brain vascularization [likely by upregulating angiogenic molecules such as VEGF (Iyer *et al*, 1998; Ryan *et al*, 2000)]. The resultant increased oxygenation then lowers HIF-1α levels, which in turn facilitates RG differentiation in a feedback (see scheme in Fig EV5J).

Our genetic studies reveal that reduced HIF-1α levels in the developing cortex *promote*—not *impair*—neurogenic differentiation of RGs, at the expense of their expansion, while increased HIF-1α levels (specifically in RGs) delayed the switch to RG differentiation and increased their expansion. These findings could not be inferred from previous studies as germ line HIF-1α deficiency causes embryonic lethality by E10.5, thereby precluding analysis of HIF-1α's role in cortical neurogenesis (Iyer *et al*, 1998). Further, deletion of HIF-1α in the CNS after the onset of cortical angiogenesis causes neuronal apoptosis late in gestation and adulthood (Tomita *et al*, 2003), but cortical neurogenesis in development was not altered (Wagenfuhr *et al*, 2015).

In adult mice, HIF-1α deletion in the dorsal forebrain, including in NPCs, impairs neurogenesis by reducing NPC proliferation and impeding differentiation (Mazumdar *et al*, 2010) but all previously used HIF-1α targeting strategies could not exclude effects on other niche cells (Iyer *et al*, 1998; Tomita *et al*, 2003; Mazumdar *et al*, 2010; Li *et al*, 2014). Indeed, loss of HIF-1α in adult Nestin$^+$ NPCs caused depletion of NSCs secondary to destabilization of the vascular niche (Li *et al*, 2014). In contrast, our study shows that HIF-1α haplodeficiency in the dorsal cortex does not affect the niche vasculature, yet alters RG differentiation. This, together with the finding that overexpression of HIF-1α selectively in a subset of RGs, without affecting other niche cell types, is capable of controlling RG expansion *versus* differentiation, indicates that HIF-1α regulates this process in a cell-autonomous manner in RGs. Moreover, HIF-1α induces Wnt/β-catenin signaling in adult NSCs (Mazumdar *et al*, 2010) but not in embryonic NSCs (this study).

Enhanced RG expansion after HIF-1α stabilization relies on Pfkfb3

Low oxygen levels increase NSC expansion *in vitro* in a HIF-1α-dependent manner, but the underlying mechanisms are unknown (Panchision, 2009; Mohyeldin *et al*, 2010). HIF-1α is a master regulator of glycolysis, a process used by proliferating cells for ATP production, but also for the generation of molecular building blocks to support biomass production for cell proliferation (Vander Heiden *et al*, 2009). Here, we show that HIF-1α stabilization in NPCs from Gpr124^{KO} embryos consistently increases the expression of glycolytic genes *in vivo* together with an increase in RG expansion. Data from *Drosophila* neuroblasts and cultured mammalian NPCs support a switch from glycolysis toward oxidative phosphorylation upon terminal differentiation. Moreover, the results in flies suggest that a transcriptional increase of oxidative phosphorylation genes is required for neuronal differentiation (Homem *et al*, 2014). In contrast, our data show downregulation of glycolytic genes in differentiated Prom1$^-$ NPC progeny compared to Prom1$^+$ NPCs in the developing mammalian cortex and reduced production of lactate—the end product of anaerobic glycolysis—at the onset of neurogenesis *in vitro*. Interestingly, we found that oxidative phosphorylation in NSCs was high and comparable to that in cortical neurons (De Bock *et al*, 2013), suggesting that embryonic NSCs—at least *in vitro*—do not increase oxidative phosphorylation, but reduce glycolysis upon differentiation. Furthermore, we show that Pfkfb3 maintains glycolysis in cortical NPCs *in vitro* and provide for the first time genetic evidence *in vivo* that expression of this glycolytic activator is critical to prevent precocious RG differentiation in the normal cortex and that increased RG expansion after HIF-1α stabilization depends on Pfkfb3. Thus, our data strongly suggest that glycolytic activity levels play an important role for RG differentiation in the mammalian cortex and that Pfkfb3-driven glycolysis is an important novel functional mediator of increased RG expansion after HIF-1α stabilization *in vivo*.

Possible implications

Direct manipulation of tissue oxygen levels specifically in the brain is currently not feasible, and exposure of pregnant dams to low ambient oxygen levels to induce tissue hypoxia causes embryonic morbidity (Ream *et al*, 2008; Wagenfuhr *et al*, 2015). We therefore used vessel-specific deficiency of GPR124 to prevent tissue oxygenation in the developing cortex by specifically perturbing brain angiogenesis. However, our findings might be relevant for pathological conditions, characterized by reduced perfusion of the developing cortex, as occurs in the hypoplastic left heart syndrome, a congenital heart disease in humans, which delays cortical gyri formation (Clouchoux *et al*, 2013; Sun *et al*, 2015), a process that directly depends on the regulation of NPCs and neurogenesis (Reillo *et al*, 2011).

Materials and Methods

Animals

Experimental animal procedures were approved by the Institutional Animal Care and Research Advisory Care Committees of the KU Leuven, Belgium; the Landesdirektion Dresden, Germany; and Stanford University, USA. *Gpr124^{KO}* (Gpr124^{tm1Cjku}) mice, *Gpr124$^{lox/lox}$* (Gpr124^{tm2Cjku}) mice, *PDGFB-Cre^{ERT2}* (Tg(Pdgfb-icre/ERT2)1Frut) mice, *Tis21*-GFP (Tis21+/$^{tm2(Gfp)Wbh}$) mice, *Emx1-Cre* (B6.129S2-*Emx1*$^{tm1(cre)Krj}$/J) mice, and *HIF-1α$^{lox/lox}$* (B6.129-*Hif1a*^{tm3Rsjo}/J) mice were previously described (Ryan *et al*, 2000; Gorski *et al*, 2002; Haubensak *et al*, 2004; Claxton *et al*, 2008; Kuhnert *et al*, 2010). For Gpr124^{KO} mice, both WT and heterozygous littermate embryos were used as control. Timed-pregnant ferrets were obtained from Marshall BioResources and housed at facilities of BioCrea GmbH (Radebeul, Dresden). At E20, E24, or E28, pregnant ferrets were anesthetized by intramuscular injection of ketamine (20 mg/kg of body weight, Bela-Pharm) and xylazine (1 mg/kg, Pharma-Partner) and euthanized by intracardiac injection of T-61 (0.3 ml/kg of body weight, Intervet), followed by the immediate removal of embryos and dissection of whole heads (E20) or brains (E24, E28) in PBS and immediate fixation.

Histology and immunohistochemistry

Mouse or ferret embryos were dissected, eventually the brain removed and fixed with 4% paraformaldehyde (PFA) overnight at 4°C. Coronal sections of the forebrain were cut at 7, 12, 20, 40, or

 © 2016 The Authors

50 μm thickness. Immunohistochemical staining was performed as described (Lange *et al*, 2009). Sections were subsequently incubated with fluorophore-conjugated secondary antibodies (Molecular Probes, Alexa-488 or Alexa-568) or with peroxidase-labeled IgGs (DAKO), followed by amplification with tyramide signal amplification system (FITC, PerkinElmer, LifeSciences) for anti-CD31, anti-HIF-1α, and anti-Glut1. HIF-1α staining required 30 min pretreatment with 1 M HCl. Blood vessels were also visualized through binding of Alexafluor 647-coupled isolectin B4 (IB4). Further details on imaging and image quantification are available in the Appendix.

qRT–PCR

RNA from cells or microdissected tissue was extracted using the Pure Link RNA Kit (Invitrogen), and genomic DNA was digested. Complementary DNA was synthetized by the QuantiTect Retrotranscriptase reaction (Qiagen). RNA expression analysis was performed by TaqMan quantitative RT–PCR on a 7500 Fast Real time PCR instrument using premade primer sets (IDT or AB Biosciences). Assay codes are available in the Appendix Table S1.

Data deposition

RNA sequencing raw data are available in the ArrayExpress database under accession number E-MTAB-3941.

Statistics

Data represent mean ± SEM of all experiments. Statistical significance was calculated by standard *t*-test or one-way ANOVA with Bonferroni *post hoc* test for more than two conditions (GraphPad Prism v5.0d). $P < 0.05$ was considered statistically significant. "*N*" defines the number of individual embryos analyzed. For the analysis of gene expression of freshly sorted cells, "*N*" defines the number of individual samples, each derived from 2 to 8 pooled littermate embryos of the same genotype. For quantification of immunohistochemistry, for each embryo, at least 500 cells in 2–6 non-consecutive sections were counted. Images were acquired and quantified blinded to the genotype of the embryos or transfected plasmids, when severity of the phenotype allowed. Otherwise, quantifications were performed by several investigators, with coherent results.

Expanded View for this article is available online.

Acknowledgements

We thank Annette Gärtner and Lieve Moons for helpful advice and discussions, Randall S Johnsson for the HIF-1α$^{lox/lox}$ mice, and Marcus Fruttiger for the Pdgfb-Cre^{ERT2} mice. We acknowledge L. Notebaert, technical staff, and VRC core facilities (VIB/KU Leuven), Jan Peychl and the Light Microscopy Facility (MPI-CBG) for their excellent assistance, as well as Barbara Langen and the staff at BioCrea GmbH and Jussi Helppi and the staff of the BioMedical Services (MPI-CBG), for housing and care of experimental animals. CL was supported by an EMBO postdoctoral fellowship. CL, HZ, and AQ are postdoctoral or predoctoral fellows, respectively, of the Research Foundation–Flanders (FWO). ID and FB are supported by a Marie Curie fellowship. This work was supported by the Belgian Science Policy (grant IAP-P6/20 and IAP-P7/20 to MD). CJK was supported by NIH R01NS064517 and R01CA158528. The work of PC is supported by the Belgian Science Policy (IAP P7/03), long-term structural Methusalem funding by the Flemish Government, grants from the FWO (G.0595.12N, 1.5.149.13N, 1.5.211.14N), the Foundation Leducq Transatlantic Network (ARTEMIS), a European Research Council (ERC) Advanced Research Grant (EU-ERC269073) and an AXA Research grant.

Author contributions

CL and PC conceptualized and CL conducted the project. CL, MTG, ID, FB, AQ, GE, RB, HZ, BB, CW, and JC performed experiments and analyzed the data. CL, MTG, GE, FLN, DL, MD, CJK, and PC designed experiments. WBH advised MTG and with CJK provided mice and expertise. CL and PC wrote the manuscript. All authors edited the paper.

Conflict of interest

The authors declare that they have no conflict of interest.

References

Anderson KD, Pan L, Yang XM, Hughes VC, Walls JR, Dominguez MG, Simmons MV, Burfeind P, Xue Y, Wei Y, Macdonald LE, Thurston G, Daly C, Lin HC, Economides AN, Valenzuela DM, Murphy AJ, Yancopoulos GD, Gale NW (2011) Angiogenic sprouting into neural tissue requires Gpr124, an orphan G protein-coupled receptor. *Proc Natl Acad Sci USA* 108: 2807 – 2812

Bartesaghi S, Graziano V, Galavotti S, Henriquez NV, Betts J, Saxena J, Deli A, Karlsson A, Martins LM, Capasso M, Nicotera P, Brandner S, De Laurenzi V, Salomoni P (2015) Inhibition of oxidative metabolism leads to p53 genetic inactivation and transformation in neural stem cells. *Proc Natl Acad Sci USA* 112: 1059 – 1064

Bjornsson CS, Apostolopoulou M, Tian Y, Temple S (2015) It takes a village: constructing the neurogenic niche. *Dev Cell* 32: 435 – 446

Britz O, Mattar P, Nguyen L, Langevin LM, Zimmer C, Alam S, Guillemot F, Schuurmans C (2006) A role for proneural genes in the maturation of cortical progenitor cells. *Cereb Cortex* 16(Suppl. 1): i138 – i151

Claxton S, Kostourou V, Jadeja S, Chambon P, Hodivala-Dilke K, Fruttiger M (2008) Efficient, inducible Cre-recombinase activation in vascular endothelium. *Genesis* 46: 74 – 80

Cleaver O, Dor Y (2012) Vascular instruction of pancreas development. *Development* 139: 2833 – 2843

Clouchoux C, du Plessis AJ, Bouyssi-Kobar M, Tworetzky W, McElhinney DB, Brown DW, Gholipour A, Kudelski D, Warfield SK, McCarter RJ, Robertson RL Jr, Evans AC, Newburger JW, Limperopoulos C (2013) Delayed cortical development in fetuses with complex congenital heart disease. *Cereb Cortex* 23: 2932 – 2943

Cullen M, Elzarrad MK, Seaman S, Zudaire E, Stevens J, Yang MY, Li X, Chaudhary A, Xu L, Hilton MB, Logsdon D, Hsiao E, Stein EV, Cuttitta F, Haines DC, Nagashima K, Tessarollo L, St Croix B (2011) GPR124, an orphan G protein-coupled receptor, is required for CNS-specific vascularization and establishment of the blood-brain barrier. *Proc Natl Acad Sci USA* 108: 5759 – 5764

De Bock K, Georgiadou M, Schoors S, Kuchnio A, Wong BW, Cantelmo AR, Quaegebeur A, Ghesquiere B, Cauwenberghs S, Eelen G, Phng LK, Betz I, Tembuyser B, Brepoels K, Welti J, Geudens I, Segura I, Cruys B, Bifari F, Decimo I *et al* (2013) Role of PFKFB3-driven glycolysis in vessel sprouting. *Cell* 154: 651 – 663

Delgado AC, Ferron SR, Vicente D, Porlan E, Perez-Villalba A, Trujillo CM, D'Ocon P, Farinas I (2014) Endothelial NT-3 delivered by vasculature and

© 2016 The Authors

CSF promotes quiescence of subependymal neural stem cells through nitric oxide induction. *Neuron* 83: 572 – 585

Dermietzel R, Krause D, Kremer M, Wang C, Stevenson B (1992) Pattern of glucose transporter (Glut 1) expression in embryonic brains is related to maturation of blood-brain barrier tightness. *Dev Dyn* 193: 152 – 163

Englund C, Fink A, Lau C, Pham D, Daza RA, Bulfone A, Kowalczyk T, Hevner RF (2005) Pax6, Tbr2, and Tbr1 are expressed sequentially by radial glia, intermediate progenitor cells, and postmitotic neurons in developing neocortex. *J Neurosci* 25: 247 – 251

Farkas LM, Haffner C, Giger T, Khaitovich P, Nowick K, Birchmeier C, Paabo S, Huttner WB (2008) Insulinoma-associated 1 has a panneurogenic role and promotes the generation and expansion of basal progenitors in the developing mouse neocortex. *Neuron* 60: 40 – 55

Franco SJ, Muller U (2013) Shaping our minds: stem and progenitor cell diversity in the mammalian neocortex. *Neuron* 77: 19 – 34

Goldman SA, Chen Z (2011) Perivascular instruction of cell genesis and fate in the adult brain. *Nat Neurosci* 14: 1382 – 1389

Gorski JA, Talley T, Qiu M, Puelles L, Rubenstein JL, Jones KR (2002) Cortical excitatory neurons and glia, but not GABAergic neurons, are produced in the Emx1-expressing lineage. *J Neurosci* 22: 6309 – 6314

Gotz M, Huttner WB (2005) The cell biology of neurogenesis. *Nat Rev Mol Cell Biol* 6: 777 – 788

Haigh JJ, Morelli PI, Gerhardt H, Haigh K, Tsien J, Damert A, Miquerol L, Muhlner U, Klein R, Ferrara N, Wagner EF, Betsholtz C, Nagy A (2003) Cortical and retinal defects caused by dosage-dependent reductions in VEGF-A paracrine signaling. *Dev Biol* 262: 225 – 241

Haubensak W, Attardo A, Denk W, Huttner WB (2004) Neurons arise in the basal neuroepithelium of the early mammalian telencephalon: a major site of neurogenesis. *Proc Natl Acad Sci USA* 101: 3196 – 3201

Homem CC, Steinmann V, Burkard TR, Jais A, Esterbauer H, Knoblich JA (2014) Ecdysone and mediator change energy metabolism to terminate proliferation in Drosophila neural stem cells. *Cell* 158: 874 – 888

Iyer NV, Kotch LE, Agani F, Leung SW, Laughner E, Wenger RH, Gassmann M, Gearhart JD, Lawler AM, Yu AY, Semenza GL (1998) Cellular and developmental control of O2 homeostasis by hypoxia-inducible factor 1 alpha. *Genes Dev* 12: 149 – 162

Javaherian A, Kriegstein A (2009) A stem cell niche for intermediate progenitor cells of the embryonic cortex. *Cereb Cortex* 19 (Suppl. 1): i70 – i77.

Jiang BH, Zheng JZ, Leung SW, Roe R, Semenza GL (1997) Transactivation and inhibitory domains of hypoxia-inducible factor 1alpha. Modulation of transcriptional activity by oxygen tension. *J Biol Chem* 272: 19253 – 19260

Jin K, Zhu Y, Sun Y, Mao XO, Xie L, Greenberg DA (2002) Vascular endothelial growth factor (VEGF) stimulates neurogenesis in vitro and in vivo. *Proc Natl Acad Sci USA* 99: 11946 – 11950

Johansson PA, Cappello S, Gotz M (2010) Stem cells niches during development-lessons from the cerebral cortex. *Curr Opin Neurobiol* 20: 400 – 407

Kim EJ, Hori K, Wyckoff A, Dickel LK, Koundakjian EJ, Goodrich LV, Johnson JE (2011) Spatiotemporal fate map of neurogenin1 (Neurog1) lineages in the mouse central nervous system. *J Comp Neurol* 519: 1355 – 1370

Kippin TE, Martens DJ, van der Kooy D (2005) p21 loss compromises the relative quiescence of forebrain stem cell proliferation leading to exhaustion of their proliferation capacity. *Genes Dev* 19: 756 – 767

Kirby ED, Kuwahara AA, Messer RL, Wyss-Coray T (2015) Adult hippocampal neural stem and progenitor cells regulate the neurogenic niche by secreting VEGF. *Proc Natl Acad Sci USA* 112: 4128 – 4133

Kriegstein A, Alvarez-Buylla A (2009) The glial nature of embryonic and adult neural stem cells. *Annu Rev Neurosci* 32: 149 – 184

Kuhnert F, Mancuso MR, Shamloo A, Wang HT, Choksi V, Florek M, Su H, Fruttiger M, Young WL, Heilshorn SC, Kuo CJ (2010) Essential regulation of CNS angiogenesis by the orphan G protein-coupled receptor GPR124. *Science* 330: 985 – 989

Lange C, Huttner WB, Calegari F (2009) Cdk4/cyclinD1 overexpression in neural stem cells shortens G1, delays neurogenesis, and promotes the generation and expansion of basal progenitors. *Cell Stem Cell* 5: 320 – 331

Li L, Candelario KM, Thomas K, Wang R, Wright K, Messier A, Cunningham LA (2014) Hypoxia inducible factor-1alpha (HIF-1alpha) is required for neural stem cell maintenance and vascular stability in the adult mouse SVZ. *J Neurosci* 34: 16713 – 16719

Mazumdar J, O'Brien WT, Johnson RS, LaManna JC, Chavez JC, Klein PS, Simon MC (2010) O2 regulates stem cells through Wnt/beta-catenin signalling. *Nat Cell Biol* 12: 1007 – 1013

Miyama S, Takahashi T, Nowakowski RS, Caviness VS Jr (1997) A gradient in the duration of the G1 phase in the murine neocortical proliferative epithelium. *Cereb Cortex* 7: 678 – 689

Mohyeldin A, Garzon-Muvdi T, Quinones-Hinojosa A (2010) Oxygen in stem cell biology: a critical component of the stem cell niche. *Cell Stem Cell* 7: 150 – 161

Noctor SC, Scholnicoff NJ, Juliano SL (1997) Histogenesis of ferret somatosensory cortex. *J Comp Neurol* 387: 179 – 193

Ottone C, Krusche B, Whitby A, Clements M, Quadrato G, Pitulescu ME, Adams RH, Parrinello S (2014) Direct cell-cell contact with the vascular niche maintains quiescent neural stem cells. *Nat Cell Biol* 16: 1045 – 1056

Panchision DM (2009) The role of oxygen in regulating neural stem cells in development and disease. *J Cell Physiol* 220: 562 – 568

Pierfelice T, Alberi L, Gaiano N (2011) Notch in the vertebrate nervous system: an old dog with new tricks. *Neuron* 69: 840 – 855

Pilaz LJ, Patti D, Marcy G, Ollier E, Pfister S, Douglas RJ, Betizeau M, Gautier E, Cortay V, Doerflinger N, Kennedy H, Dehay C (2009) Forced G1-phase reduction alters mode of division, neuron number, and laminar phenotype in the cerebral cortex. *Proc Natl Acad Sci USA* 106: 21924 – 21929

Raab S, Beck H, Gaumann A, Yuce A, Gerber HP, Plate K, Hammes HP, Ferrara N, Breier G (2004) Impaired brain angiogenesis and neuronal apoptosis induced by conditional homozygous inactivation of vascular endothelial growth factor. *Thromb Haemost* 91: 595 – 605

Ramasamy SK, Kusumbe AP, Adams RH (2015) Regulation of tissue morphogenesis by endothelial cell-derived signals. *Trends Cell Biol* 25: 148 – 157

Ream M, Ray AM, Chandra R, Chikaraishi DM (2008) Early fetal hypoxia leads to growth restriction and myocardial thinning. *Am J Physiol Regul Integr Comp Physiol* 295: R583 – R595

Reillo I, de Juan Romero C, Garcia-Cabezas MA, Borrell V (2011) A role for intermediate radial glia in the tangential expansion of the mammalian cerebral cortex. *Cereb Cortex* 21: 1674 – 1694

Ryan HE, Poloni M, McNulty W, Elson D, Gassmann M, Arbeit JM, Johnson RS (2000) Hypoxia-inducible factor-1alpha is a positive factor in solid tumor growth. *Cancer Res* 60: 4010 – 4015

Shah SR, Esni F, Jakub A, Paredes J, Lath N, Malek M, Potoka DA, Prasadan K, Mastroberardino PG, Shiota C, Guo P, Miller KA, Hackam DJ, Burns RC, Tulachan SS, Gittes GK (2011) Embryonic mouse blood flow and oxygen correlate with early pancreatic differentiation. *Dev Biol* 349: 342 – 349

Shen Q, Goderie SK, Jin L, Karanth N, Sun Y, Abramova N, Vincent P, Pumiglia K, Temple S (2004) Endothelial cells stimulate self-renewal and expand neurogenesis of neural stem cells. *Science* 304: 1338 – 1340

Siegenthaler JA, Ashique AM, Zarbalis K, Patterson KP, Hecht JH, Kane MA, Folias AE, Choe Y, May SR, Kume T, Napoli JL, Peterson AS, Pleasure SJ

 © 2016 The Authors

(2009) Retinoic acid from the meninges regulates cortical neuron generation. *Cell* 139: 597 – 609

Stubbs D, Deproto J, Nie K, Englund C, Mahmud I, Hevner R, Molnar Z (2009) Neurovascular congruence during cerebral cortical development. *Cereb Cortex* 19: i32 – i41

Sun T, Hevner RF (2014) Growth and folding of the mammalian cerebral cortex: from molecules to malformations. *Nat Rev Neurosci* 15: 217 – 232

Sun L, Macgowan CK, Sled JG, Yoo SJ, Manlhiot C, Porayette P, Grosse-Wortmann L, Jaeggi E, McCrindle BW, Kingdom J, Hickey E, Miller S, Seed M (2015) Reduced fetal cerebral oxygen consumption is associated with smaller brain size in fetuses with congenital heart disease. *Circulation* 131: 1313 – 1323

Tomita S, Ueno M, Sakamoto M, Kitahama Y, Ueki M, Maekawa N, Sakamoto H, Gassmann M, Kageyama R, Ueda N, Gonzalez FJ, Takahama Y (2003) Defective brain development in mice lacking the Hif-1alpha gene in neural cells. *Mol Cell Biol* 23: 6739 – 6749

Urban N, Guillemot F (2014) Neurogenesis in the embryonic and adult brain: same regulators, different roles. *Front Cell Neurosci* 8: 396

Vander Heiden MG, Cantley LC, Thompson CB (2009) Understanding the Warburg effect: the metabolic requirements of cell proliferation. *Science* 324: 1029 – 1033

Wagenfuhr L, Meyer AK, Braunschweig L, Marrone L, Storch A (2015) Brain oxygen tension controls the expansion of outer subventricular zone-like basal progenitors in the developing mouse brain. *Development* 142: 2904 – 2915

Wang W, Osenbroch P, Skinnes R, Esbensen Y, Bjoras M, Eide L (2010) Mitochondrial DNA integrity is essential for mitochondrial maturation during differentiation of neural stem cells. *Stem Cells* 28: 2195 – 2204

Weigmann A, Corbeil D, Hellwig A, Huttner WB (1997) Prominin, a novel microvilli-specific polytopic membrane protein of the apical surface of epithelial cells, is targeted to plasmalemmal protrusions of non-epithelial cells. *Proc Natl Acad Sci USA* 94: 12425 – 12430

Zhou Y, Nathans J (2014) Gpr124 controls CNS angiogenesis and blood-brain barrier integrity by promoting ligand-specific canonical wnt signaling. *Dev Cell* 31: 248 – 256

© 2016 The Authors